Astronomy & Astrophysics manuscript no. Ha3˙data˙rev3
March 6, 2013

© ESO 2013

arXiv:1206.0061v1 [astro-ph.CO] 1 Jun 2012

Hα3: an Hα imaging survey of HI selected galaxies from ALFALFA[⋆]

I: Catalogue in the Local Supercluster

G. Gavazzi[1], M. Fumagalli[2], V. Galardo[1], F. Grossetti[1], A. Boselli[3], R. Giovanelli[4], M.P. Haynes[4], and S. Fabello[5]

[1] Università degli Studi di Milano-Bicocca, Piazza della Scienza 3, 20126 Milano, Italy
e-mail: `giuseppe.gavazzi@mib.infn.it`
[2] Department of Astronomy and Astrophysics, University of California, 1156 High Street, Santa Cruz, CA 95064, USA
e-mail: `mfumagalli@ucolick.org`
[3] Laboratoire d'Astrophysique de Marseille, UMR 6110 CNRS, 38 rue F. Joliot-Curie, F-13388, Marseille, France
e-mail: `alessandro.boselli@oamp.fr`
[4] Center for Radiophysics and Space Research, Space Science Building, Ithaca, NY, 14853
e-mail: `haynes@astro.cornell.edu, riccardo@astro.cornell.edu`
[5] Max Planck Institute for Astrophysics, Garching, Karl-Schwarzschild-Str. 1, Postfach 1317, D-85741 Garching, Germany
e-mail: `fabello@mpa-garching.mpg.de`

Received December 15, 2009; accepted

ABSTRACT

Context. We present Hα3 (acronym for H$\alpha - \alpha\alpha$), an Hα narrow-band imaging survey of ∼ 400 galaxies selected from the HI Arecibo Legacy Fast ALFA Survey (ALFALFA) in the Local Supercluster, including the Virgo cluster.
Aims. By using hydrogen recombination lines as a tracer of recent star formation, we aim to investigate the relationships between atomic neutral gas and newly formed stars in different environments (cluster and field), morphological types (spirals and dwarfs), and over a wide range of stellar masses ($\sim 10^{7.5} - 10^{11.5}$ M$_\odot$).
Methods. We image in Hα+[NII] all the galaxies that contain more than 10^7 M$_\odot$ of neutral atomic hydrogen in the sky region 11^h < R.A. < 16^h; 4^o < Dec. < 16^o; 350 <cz< 2000 km s^{-1} using the San Pedro Martir 2m telescope. This survey provides a complete census of the star formation in HI rich galaxies of the local universe.
Results. We present the properties of the galaxy sample, together with Hα fluxes and equivalent widths. We find an excellent agreement between the fluxes determined from our images in apertures of 3 arcsec diameter and the fluxes derived from the SDSS spectral database. From the Hα fluxes corrected for galactic and internal extinction and for [NII] contamination we derive the global star formation rates (SFRs).

Key words. Galaxies: clusters: individual: Virgo – Galaxies: fundamental parameters *colors, luminosities, masses* – Galaxies: ISM

1. Introduction

The large amount of multi-wavelength data from recent and ongoing surveys is providing a wealth of information on the different phases of the interstellar medium (ISM), the stellar content and the present day star formation rates (SFRs) in nearby galaxies. Complemented with results from numerical simulations and theory, these observations contribute to our understanding of the basic process that regulates the life of a galaxy: the conversion of gas into stars. However, crucial questions remain open on which gas phase (on which scale) is ultimately responsible for new star formation, on which tracers for the SFR are unbiased, and on the role of very massive stars and of the environment in shaping what is the observed luminosity in local galaxies.

Half a century has passed since Schmidt (1959) discovered a foundamental relation between the surface density of the star formation and that of the gaseous component in galaxies[1], today known as the Kennicutt-Schmidt (KS) law (Schmidt 1959, Kennicutt 1989, 1998). Since then, a large number of theoretical and observational studies have addressed the origin of this correlation. Modern observations reveal a relation between molecular gas and star formation rate surface density (Wong & Blitz 2002, Kennicutt et al. 2007, Bigiel et al. 2008) within the optical radius where CO seems to be a reliable tracer of molecular hydrogen. While this contrasts the original form of the KS law in which a correlation between the SFR and the much more extended atomic gas is evident over several order of magnitude in SFR, this finding is consistent with the basic picture of star formation in giant molecular clouds. But it is unclear whether molecular hydrogen drives this correlation (Krumholz et al. 2011, Glover & Clark 2011) and departures from this observed relation are still a matter of debate (Fumagalli & Gavazzi 2008, Bigiel et al. 2010, Schruba et al. 2011).

Whereas there is unanimous consent that high luminosity late-type galaxies display low specific star formation rate (SSFR), i.e. SFR per unit stellar mass, as expected from *downsizing* (e.g. Gavazzi et al. 1996), the behavior of dwarf galaxies, whose SSFR spans a range exceeding two orders of magnitude (Lee et al. 2007), is poorly understood. In addition, the SFR inferred from the Hα hydrogen recombination line in these systems or in the outskirt of disks, systematically underpredicts the

---

[⋆] Observations taken at the observatory of San Pedro Martir (Baja California, Mexico), belonging to the Mexican Observatorio Astronómico Nacional.

[1] The 50th anniversary from the original Schmidt (1959) paper was celebrated during the conference SFR@50 held in Spineto in 2009

one derived from the UV light (Meurer et al. 2009, Lee et al. 2009) to the point that doubts have been cast on the universality of the initial mass function (IMF; e.g. Meurer et al. 2009) and on the reliability of hydrogen recombination lines to trace star formation (Pflamm-Altenburg et al. 2007). However, uncertainties in the dust extinction (Boselli et al. 2009), star formation history (Weisz et al. 2011) and a stochastic star formation rate (Fumagalli et al. 2011) can explain equally well the observed luminosity even for a universal IMF.

Similarly, the debate on the role of the environment in shaping the star formation properties of galaxies is still open (see a review by Boselli & Gavazzi 2006). While it is observed that atomic (e.g. Gavazzi et al. 2002b, Cortese & Hughes 2009, Rose et al. 2010) and, in highly perturbed systems, molecular (Vollmer et al. 2008, Fumagalli et al.2009, Vollmer et al. 2009) gas depletion result in a low level of star formation, simulations of ram-pressure stripping have suggested different degrees of enhancement in the SFR of perturbed galaxies (e.g. Kronberger et al. 2008, Kapferer et al. 2009, Tonnesen & Bryan 2009). And studies of the Hα morphology in galaxies within rich groups of clusters show a mix of global suppression and truncation of the Hα disks (Vogt et al. 2004, Koopmann & Kenney 2004, Fumagalli & Gavazzi 2008, Welikala et al. 2008, Rose et al. 2010), but a definitive assessment of the relative importance of these different perturbations is still lacking.

To address some of these open issues, we have recently completed Hα3, an Hα narrow-band imaging survey at the 2.1m telescope of the San Pedro Martir (SPM) Observatory. Our sample includes $\sim$ 400 nearby galaxies, selected from the ongoing blind HI Arecibo Legacy Fast ALFA Survey (ALFALFA; Giovanelli et al. 2005) in the Spring sky of the Local Supercluster, including the Virgo cluster, in the velocity window $350 < cz < 2000$ km s^{-1}. Together with ancillary multifrequency data and complemented by similar surveys (Meurer et al. 2006) or with optically selected samples (James et al. 2004, Kent et al. 2008), these observations provide a complete census of the SFR in the local universe traced by hydrogen recombination lines (see also Bothwell et al. 2009).

The present paper, first of a series, presents the basic properties of the Hα3 dataset in the Local Supercluster (Sect. 2). After a description of observations (Sect. 3) and data reduction (Sect. 4), we list previously unpublished Hα fluxes and equivalent widths for 235 galaxies. Summary and future prospects follow in Sect. 5, while in Appendix B we give an Atlas of the images of the sampled galaxies.

Paper II of this series will contain the analysis of the integrated quantities (global SFR) produced by Hα3 in the Local Supercluster, and will investigate the relationships between atomic neutral gas and newly formed stars in different environments (cluster and field), morphological types (spirals and dwarfs), and over a wide range of stellar masses ($\sim 10^{7.5} - 10^{11.5}$ M$_\odot$).

Paper III will contain the extension of Hα3 to the Coma Supercluster ($10^h < $ R.A. $< 16^h$; $24^o <$ Dec. $< 28^o$; $3900 <$ cz < 9000 km s^{-1}).

The analysis of the Hα morphology from Hα3 in both the Local and the Coma Superclusters will be carried out in Paper IV, which will address the comparison of the effective radii at Hα and r band as a function of morphological type, and the determination of other structural parameters such as the Concentration index, the Asymmetry and the Clumpiness parameters introduced by Conselice (2003). Throughout the paper we adopt $H_0 = 73$ km s^{-1} Mpc^{-1}.

2. The Sample

2.1. Selection

Our sample is drawn from the 900 square degree region $11^h <$ R.A. $< 16^h$; $4^o <$ Dec. $< 16^o$; $350 < cz < 2000$ km s^{-1}, covering the Local Supercluster, including the Virgo cluster[2]. This region has been fully mapped by ALFALFA that is providing us with a complete sample of HI selected galaxies, with masses as low as $10^{6.5-7.0}$ $M_\odot$, 7.7 times deeper than HIPASS, the HI Parkes All-Sky Survey (Meyer et al. 2004)[3]. The most comprehensive catalogue containing 40% of the entire ALFALFA coverage is given in Haynes et al. (2011), superseding previous ALFALFA publications (e.g. Giovanelli et al. 2007) for region $11^h44^m <$ R.A. $< 14^h00^m$; $12^o <$ Dec. $< 16^o$, and Kent et al. (2008) for region $11^h26^m <$ R.A. $< 13^h52^m$; $4^o <$ Dec. $< 12^o$).

The goal of the Hα3 survey is to follow up with Hα imaging observations the ALFALFA targets with high S/N (typically S/N > 6.5) and good match between two independent passes (code = 1 sources; Giovanelli et al. 2005 and Haynes et al. 2011). In addition, we limit to objects with HI fluxes $F_{\rm HI} > 0.7$ Jy km s^{-1}. At the distance of 17 Mpc, assumed for the Virgo cluster, a flux limit $F_{\rm HI} = 0.7$ Jy km s^{-1} corresponds to a HI mass $M_{\rm HI} = 10^{7.7}$ M$_\odot$.

Figure 1 illustrates the sky region under study. The bottom panel contains the 383 sources that have been observed in Hα. In addition, 26 sources in the Virgo cluster (big open circles) were observed in spite of having $F_{\rm HI} < 0.7$ Jy km s^{-1} and hence not strictly belonging to the Hα3 sample selection. This brings the total number of observed galaxies to 409.

2.2. Completeness

The top panel of Figure 1 shows 68 ALFALFA sources that have not been observed by Hα3. Among them, 38 (triangles) do not have any optical counterpart because they are either debris of ram pressure stripped gas (Kent et al. 2007) or too faint in optical light to be visible on SDSS plates. These would have been undetected for the typical exposure time of our survey (see Sect. 4). Of the remaining, 8 galaxies (squares) are close to bright stars whose charge bleeding would have destroyed the requested photometric accuracy. Finally, 20 galaxies will be considered in future runs (crosses). After accounting for these missing sources, the completeness yet achieved is 87% in Virgo and 82% outside, normalized to the ALFALFA catalogue. To further investigate the HI completeness of Hα3, i.e. the limiting HI mass above which Hα3 is complete, we compare in Fig. 2 the ALFALFA HI mass function given by Martin et al. (2010) (black line), representative of the whole Local Universe sampled by ALFALFA, which is well represented by a Schechter function with α=-1.33,

---

[2] The lower velocity limit is dictated by the fact that none of interferometric filters available at SPM covers the Hα line for redshift $<$ 350 km s^{-1}. Furthermore some galaxies have been serendipitously observed in spite of having $cz > 2000$ km s^{-1}, but they do not constitute a complete sample. In the Virgo cluster however we extend the velocity coverage of Hα3 to $350 <$ cz < 3000 km s^{-1} in order to include the finger of God of the cluster in its full extent (Gavazzi et al. 1999).

[3] As introduced in Giovanelli et al. (2005) ALFALFA is a noise-limited survey rather than a flux-limited one. At any given integrated H$_{\rm I}$ mass the 21 cm flux per velocity channel is inversely proportional to the width of the H$_{\rm I}$ profile, thus to the galaxy inclination. The completeness and sensitivity of ALFALFA are well understood and discussed in detail in Saintonge (2007), Martin at al. (2010) and Haynes et al. (2011).

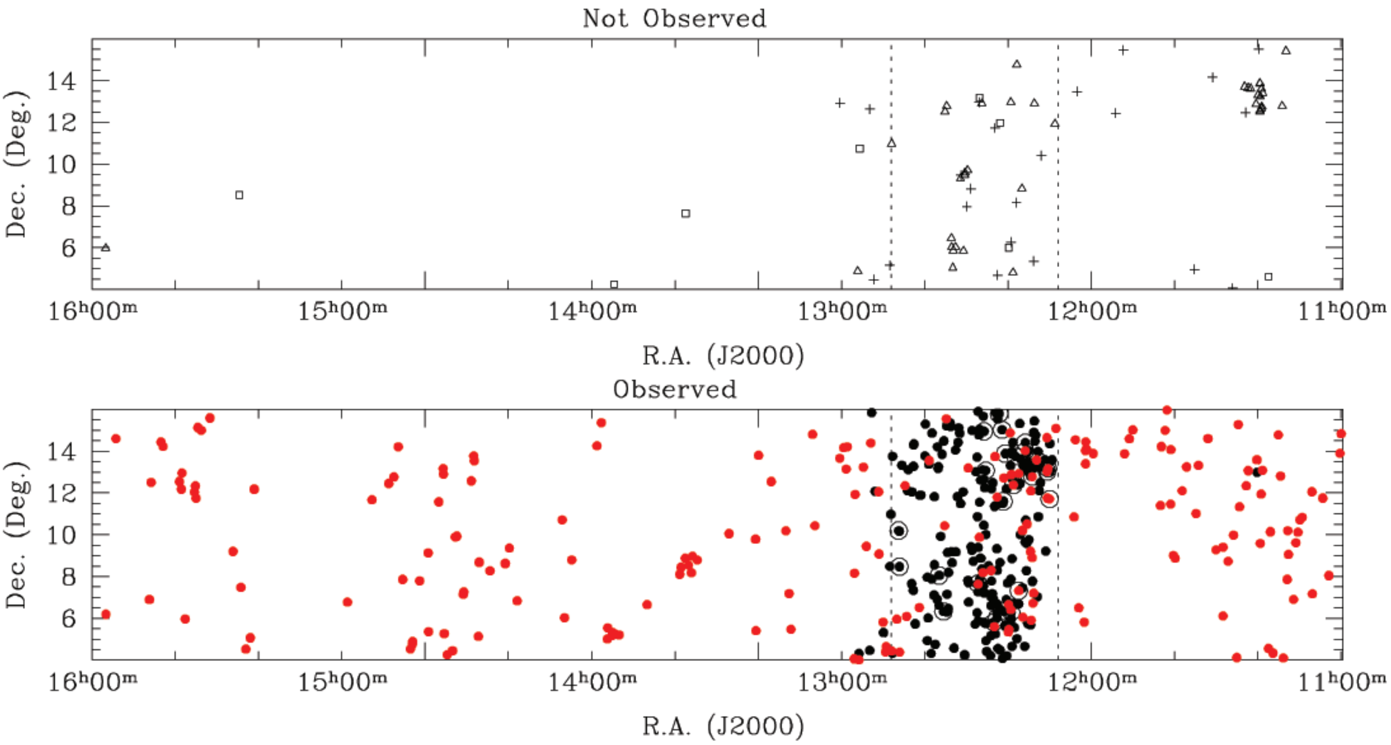

Fig. 1. Bottom panel. Sky distribution of 409 HI selected galaxies observed in the present survey, 383 with $F_{HI} > 0.7$ Jy km s^{-1} (filled circles) and 26 with < 0.7 Jy km s^{-1} (big empty circles). Red symbols refer to 233 new sources observed in 2006-2009 whose fluxes are presented in this paper. Top panel. 68 HI targets that matches our selection criteria but that were not observed because: 8 lie too close to bright stars; 38 are either debris of ram pressure stripped gas or their associated galaxy is too faint to be seen on SDSS plates (triangles); 20 that will be consider in future runs (crosses). The two vertical broken lines mark the adopted boundaries of the Virgo cluster.

$\Phi_* = 4.8 \cdot 10^{-3}$Mpc^{-3}dex^{-1}, $M_* = 10^{9.964}$ with the HI Mass distribution in Hα3 (histogram). The red curve is the ALFALFA HI mass function whose Φ_* has been normalized to the volumes sampled by Hα3, separately for Virgo and the isolated volume, to account for the overdensity in the two subsample with respect to ALFALFA. This has been done by dividing the integral of the ALFALFA HI mass function in the interval $10^{8-9.75}$ $M_\odot$ by the integral of the observed histogram in the same interval. The normalization coefficients are 1.96 (isolated), 2.99 (all), 6.01 (Virgo). The agreement between the red line and the histogram is very satisfactory above log $M_{HI} = 8$ $M_\odot$, that can be assumed as the HI completeness limit of Hα3. The data and the red line depart above log $M_{HI} = 9.75$ $M_\odot$ due to cosmic variance as the number of high HI mass galaxies sampled by Hα3 is limited. This is an effect of HI deficiency and the highest HI mass objects are too rare to be found in the small volume sampled by Hα3. The lack of objects with log $M_{HI} > 9.75$ $M_\odot$ is however only of 1-2 objects.

The optical completeness of Hα3 cannot be determined as accurately as for the HI mass because the optical luminosity function of the HI selected galaxies is unknown. However we empirically determine the optical completeness by deriving the cumulative distribution in 0.5 mag bins of i-band luminosity of galaxies in the three observed volumes: isolated, Virgo, all. The cumulative distribution flattens at $M_i > -15.25$, (corresponding to log $(M_{lim}/M_\odot) = 7.8$). This represents the i-band completeness limit of our HI selected sample that is largely composed of late-type galaxies.

2.3. Ancillary Data

The whole region of interest has been covered with imaging and spectroscopic observations by the SDSS (DR7, Abazajian et al. 2009). However, given the proximity of the surveyed galaxies, their angular size often exceeds several arcmin, making the shredding problem (Blanton et al. 2005a,b,c) that affects the pipeline of SDSS particularly severe. For this reason and owing to fiber conflict that reduces the number of galaxies with nuclear spectra, the SDSS spectral database is not fully complete/reliable for the nearby Universe ($z << 0.2$). As for example, the catalogued magnitudes are often wrong by several magnitudes. To avoid this problem, the individual g and i band SDSS images centered on each galaxy targeted by Hα3 were downloaded from the SDSS archive. Many of the large galaxies are cut in several pieces belonging to adjacent "tiles". These images were downloaded individually and combined to cover a sufficient area to contain the whole galaxies as well as some empty sky. The background was estimated and subtracted us-

---

[4] A more thorough derivation of the ALFALFA HI mass function is in Hallenbeck et al. in preparation.

ing the tasks MARKSKY and SKYSUB in IRAF[5] GALPHOT[6]. The background subtracted frames were inspected individually and background objects and foreground stars were masked when found within or near the galaxies of interest. The photometry in the edited frames was obtained using *QPHOT* in IRAF by integrating the counts within a circular aperture (determined in *i*-band) containing all the flux. This procedure provides an accurate estimate of the total *g* and *i* magnitudes (see Table B.1). During this process the major and minor diameters of the galaxies were crudely determined using elliptical regions adapted to the shape of galaxies (see Table B.1) in DS9.

The distance to the galaxies belonging to the Virgo cluster is computed according to Gavazzi et al (1999), who adopts 17 Mpc for members to Virgo A, and for the N, S, E clouds, 23 Mpc for Virgo B (M49), and 32 Mpc for clouds M and W. These values are consistent with the more modern determination obtained with the surface brightness fluctuation method on HST-ACS images by Mei at al. (2007). For all other members of the Local Supercluster we adopt the galactocentric (GSR) distances listed in NED.

The HI mass is computed using $M_{HI} = 2.36 \cdot 10^5 \cdot S_{21} \cdot D^2$, where D is the distance to the source in Mpc and S_{21} is the integrated flux under the HI profile in units of Jy-km s^{-1} from ALFALFA.

The stellar mass is derived from the *i* magnitudes and $g - i$ color using the Bell's et al. (2003) recipe: $\log M_{star} = -0.152 + 0.518 \cdot (g - i) + \log i_{lum} M_{\odot}$, where i_{lum} is the *i* band luminosity in solar units.

2.4. Optical Properties

For a large majority of the 224 Virgo galaxies (12^h05^m < R.A. < 12^h50^m ; 4° < Dec. < 16°; $cz < 3000$ km s^{-1}; black filled circles in Figure 1) the Hα data have been already published in previous papers (Gavazzi et al. 2002a; Boselli & Gavazzi 2002; Boselli et al. 2002; Gavazzi et al. 2002b; Gavazzi et al. 2006). Images and fluxes are publicly available via the GOLDMine web server (Gavazzi et al., 2003).

Properties for the 235 unpublished sources observed in the period 2006-2009 (red filled circles in Fig. 1) are presented in Table B.1. Individual entries are as it follows:

- Column 1: AGC designation, from Haynes et al. (2011). AGC numbers coincide with UGC numbers for those galaxies included in the UGC (Nilson 1973);
- Columns 2 and 3: optical celestial coordinates (J2000);
- Columns 4, 5, 6 and 7: CGCG (Zwicky et al. 1968), UGC (Nilson 1973), NGC (Dreyer 1888) and IC (Dreyer 1908) designations;
- Column 8: morphological type, from NED or classified by the authors on SDSS *i*-band images;
- Column 9: heliocentric velocity of the HI source, $cz_{\odot}$ in km s^{-1} from Haynes et al. (2011);

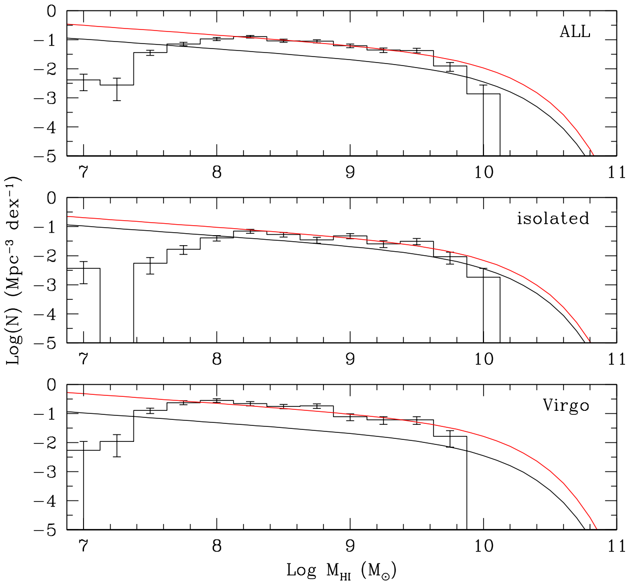

Fig. 2. Comparison of the observed HI mass distribution in the three subsamples (histograms) with the HI mass function of Martin et al. (2010) (black lines) and one corrected for the overdensity in the Local Supercluster (red lines).

- Columns 10 and 11: major an minor optical diameters from NED or measured with ellipses on SDSS *i*-band frames (see section 2.3). These are consistent with 25*th* magarcsec^{-1} isophotal diameters;
- Columns 12 and 13: *i* and *g* integrated (AB) magnitude obtained on SDSS frames (see section 2.3).
- Columns 14: adopted galactocentric (GSR) distances as given by NED (Mpc).

An overview of the sample properties is given in Figure 3. Panel (a) shows the limiting Hα fluxes, computed from the pixel to pixel 1σ sky fluctuation. We note that most of the galaxies lie in a quite narrow distribution (~ 0.15 dex), with a median Hα flux of $10^{-14.3\pm0.15}$ erg cm^{-2} sec^{-1}, revealing that Hα3 is a rather homogeneous survey, despite the fact that observations were spread over almost one decade. At the distance of Virgo, our typical sensitivity corresponds to an unobscured SFR level of 1.3×10^{-3} $M_{\odot}$ yr^{-1} at 1σ, computed as outlined in Sect. 4.3. Panel (b) shows the distribution of morphological types from the ALFALFA galaxy catalogue (dashed line) and from Hα3. Perhaps not surprisingly, an HI selected sample is strongly biased towards spirals and irregular galaxies (Gavazzi et al. 2008) at the depth achieved by ALFALFA. Stellar properties for our sample (solid lines) and for ALFALFA galaxies (dashed lines) are presented in panel (c). Owing to the correspondence between stellar masses and HI masses (e.g. Gavazzi et al. 2008), the stellar distribution resembles the one for the gas masses, with a significant completeness down to less than 10^8 $M_{\odot}$ (see Sect. 2.2). Galaxies in Hα3 span a wide range in color and gas fraction, allowing a statistical analysis of the star formation over a large space of parameters. In the color-magnitude diagram (d), HI selected galaxies lie almost exclusively in the blue cloud, while the red sequence (represented in the figure by the linear regression $g - i = -0.0585 \cdot (M_i + 16) + 0.98$; Gavazzi et al. 2010) is grossly undersampled, as evident in the color magnitude diagram (Figure 7) of Haynes et al. (2011). To detect the low level of atomic gas present in galaxies located in the green valley or even in the red sequence, deeper HI observations are required (e.g. Catinella et al. 2010). More detailed discussions of stellar and star formation properties of the ALFALFA population overall are presented in Huang et al. (2011a) and Huang et al (2011b).

---

[5] IRAF is the Image Analysis and Reduction Facility made available to the astronomical community by the National Optical Astronomy Observatories, which are operated by AURA, Inc., under contract with the U.S. National Science Foundation. STSDAS is distributed by the Space Telescope Science Institute, which is operated by the Association of Universities for Research in Astronomy (AURA), Inc., under NASA contract NAS 5–26555.

[6] developed for IRAF - STSDAS mainly by W. Freudling, J. Salzer, and M.P. Haynes (Haynes et al. 1999) and adapted by L. Cortese and S. Zibetti to handle Hα data.

3. Observations

Observations of HI selected galaxies from ALFALFA were completed in four runs of 9 nights each, allocated from 2006 to 2009 by the Mexican Observatorio Astronómico Nacional (OAN) at the San Pedro Martir Observatory (SPM, Baja California, Mexico). Owing to the excellent weather conditions which are frequently encountered at SPM in the late Spring, we were able to observe mostly in photometric conditions: 8/9 nights in 2006, 9/9 in 2007-2008 and 5/9 in 2009 During these runs[7], we focused on the field surrounding the Virgo cluster, since most of the ALFALFA sources in Virgo were already observed as part of a survey of optically selected galaxies started in 1999, using various telescopes: the OHP and Calar Alto 1.2m (Boselli & Gavazzi 2002), the INT and NOT 2.5m (Boselli et al. 2002), the ESO 3.6m (Gavazzi et al. 2006) and the SPM 2.1m (Gavazzi et al.2002a, b, 2006). We point to these papers for a detailed description of the observing strategies, data reduction and values for Hα fluxes in this subsample.

As for the data acquired between 2006 and 2009, we obtained narrow-band imaging in the Hα emission line (rest frame $\lambda = 6562.8$ Å) with the ($f/7.5$) Cassegrain focus imaging camera of the SPM 2.1 m telescope, equipped with a SIT3 1024×1024 pixels CCD detector with a pixel size of $0.31''$. The detector was used in the 1 e^{-}/ADU gain mode. The redshifted Hα line (ON-band frame) was imaged through a narrow band (λ 6603 Å, $\Delta\lambda \sim 73$ Å) interferometric filter, whose bandpass include also the [NII] lines. Except for two galaxies at lower velocities ($cz < 300$ km s^{-1}), this filter maximizes the throughput at the galaxy redshift, as shown in Fig. 4[8]. For each galaxy, we acquired multiple ON-band exposures with an integration time ranging from 15 to 60 min, according to seeing conditions and to source brightness. The stellar continuum subtraction was secured by means of shorter (typically 3 to 5 min) observations taken through a broad-band (λ 6231 Å, $\Delta\lambda \sim 1200$ Å) r-Gunn filter (OFF-band frames). While the median seeing of the San Pedro Martir site is $\sim 0.''6$, the final FWHM for point sources in the images is affected by the poor telescope guiding and dome seeing. For these reasons, the final distribution ranges from $1''$ to $\sim 2''.5$ (measured fitting a Gaussian profile to the stars), with a mean seeing of $\sigma = 1''.40 \pm 0''.28$ in the OFF-band images and $\sigma = 1''.6 \pm 0''.3$ in the longer ON-band exposures, as shown in Figure 5.

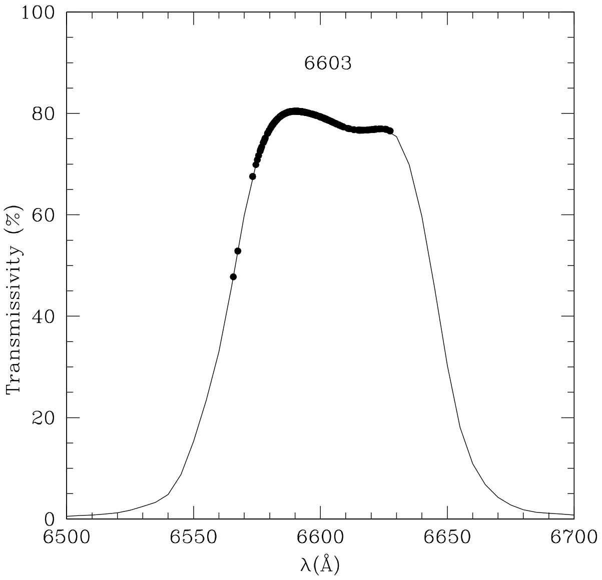

Fig. 4. The transmissivity of the ON-band (6603 Å) filter. Filled circles mark the transmissivity for $H\alpha$ at the redshift of the target galaxies. Two galaxies with cz=132 and 213 km s^{-1} have been observed on the steep shoulder of the filter transmission curve. They will not be further considered in the analysis.

We derive the absolute flux levels with reference stars Feige34 and HZ44 from the catalogue of Massey et al. (1988), observed every ~ 2 hours. Repeated measurements gave $< 5\%$ differences that we assume as the 1σ photometric uncertainty. [9] An handful number of galaxies have been imaged in transparent but not photometric conditions and for these objects we derive only the Hα equivalent width (EW; insensitive to the absolute flux level), but not the Hα flux.

We list information for individual galaxies in Table B.2, as follows:

- Column 1: AGC designation, from Haynes et al. (2011);
- Column 2: observing date (yy-mm-dd UT);
- Columns 3 and 4: duration and number of individual ON-band exposures;
- Column 5: average air mass during the ON-band exposures;
- Column 6: adopted photometric zero point;
- Column 7: FWHM of point sources (arcsec) in the ON-band frames, as measured on the images;
- Columns 8 and 9: duration and number of individual OFF-band exposures;
- Column 10: FWHM of point sources (arcsec) in the OFF-band frames, as measured on the images;
- Column 11: normalization factor n of the OFF-band frames (see next section).

4. Data Reduction

4.1. Image Analysis

We reduce the CCD frames following the procedure described Gavazzi et al. (2002b), using the STSDAS and GALPHOT IRAF packages. To compensate the spatial differences in the detector response, each image is bias subtracted and divided by the median of several flat-field exposures obtained during twilight in regions devoid of stars. When three exposures are available,

---

[7] During an unfortunate run in 2010 the SIT3 CCD broke and was substituted with an outdated Thompson detector, badly affected by fringing in the red and with a low quantum efficiency. Due to the poor weather we could observe only 2 additional galaxies that are listed at the end of the Tables.

[8] Two galaxies AGC4880 and AGC190160 with cz=4971 and 4954 km s^{-1} respectively have been observed through a filter centered at λ 6683 Å. The will not be considered in any further analysis

[9] The stability of the photometry during each runs was such that we were able to detect a zero-point decrease of 0.12 dex in 4 years due to loss of reflectivity of the mirrors.

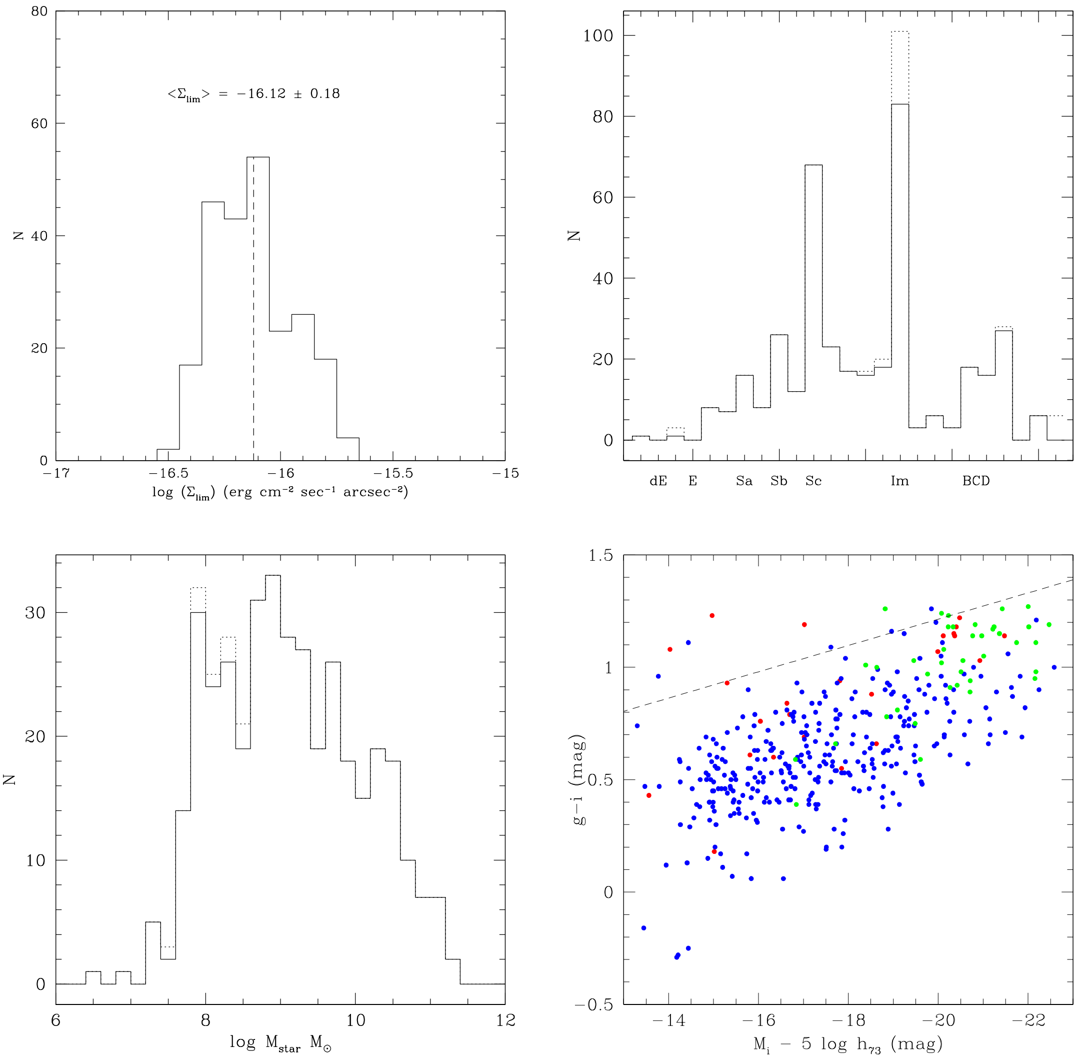

Fig. 3. Properties of the Hα3 sample, compared against the entire ALFALFA catalogue (dotted lines) and the one restricted to galaxies with optical counterparts (dashed lines). Panel (a): 1σ limiting surface brightness (erg cm^{-2} sec^{-1} arcsec^{-2}) in the Hα NET images. Panel (b): Morphological types. Panel (c): Stellar masses from *i*-band photometry. Panel (d): Color ($g - i$) magnitude (i band) diagram (color coded by morphology: red=early, blue=disk; green=bulge+disk) (SDSS magnitudes are uncorrected for internal extinction). Hα3 is a homogeneous survey, complete down to a SFR density of $3x10^{-9}$ M$_\odot$ yr^{-1} pc^{-2} (1 σ) and HI masses of 10^8 M$_\odot$. This sample spans a wide range in color, morphological type, colors and stellar masses that allows a comparison of the SFR over a broad parameter space.

we adopt a median combination of the realigned images to reject cosmic rays in the final stack. For galaxies observed in single exposures, we reject cosmic rays by direct inspection of the frames. For each frame, we subtract a mean local sky background, computed around the galaxy using the GALPHOT tasks MARKSKY and SKYFIT. Over the typical spatial scale of galaxies (50″ – 200″) the mean background varies by ∼ 10% of the sky rms per pixels. This is caused by residual patterns after flat-fielding and represents the dominant source of error in low S/N regions. Over extended objects, the inability to subtract the sky with high accuracy introduces an additional error on the final flux, which we properly account for in computing the error budget.

4.2. Integral Photometry

Due to the proximity of the two [NII] emission lines (λ 6548-6584 Å) to the Hα line, the flux measured in the ON-band observations refers to a combination of Hα+[NII]. While a proper correction for [NII] emission is required before the final SFR is computed, in this section we will generically refer to Hα as the total flux Hα+[NII].

Fluxes and EWs of the Hα line can be recovered from narrow ON-band observations by subtracting the stellar continuum contribution estimated using OFF-band images, once these are normalized to account for the ratio of the transmissivity of the two filters and the difference in exposure time. For each galaxy, we derive the normalization coefficient *n* by assuming that field stars have no significant Hα emission on average and therefore they have identical continuum levels in the ON- and OFF-band frames (see however Spector et al. 2011).

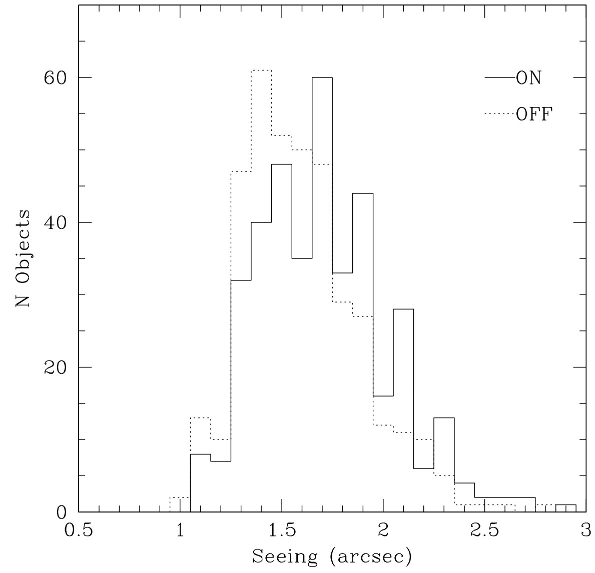

Fig. 5. Point source FWHM measured on the final ON-band images (solid histogram) and OFF-band images (dashed histogram). Poor telescope guiding performance and dome seeing affect the image quality, making the distribution of the seeing slightly better in the shorter OFF exposures.

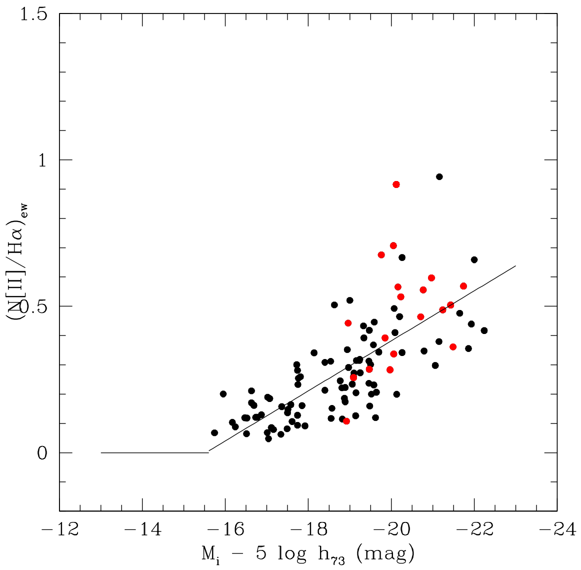

Fig. 6. The ratio $([NII]/H\alpha)_{ew}$ derived from drift-scan spectra as a function of M_i, exhibiting the variation expected for the mass-metallicity relation. Red points mark AGNs. The line indicates the linear fit to the data adopted when drift-scan spectra are unavailable.

Once the normalization coefficient is known, we derive the integrated Hα flux performing aperture photometry on both the OFF- and ON-band sky subtracted frames. First, we derive the integrated net counts C_{NET} as:

$$C_{NET} = C_{ON} - n \cdot C_{OFF}^{raw} = C_{ON} - C_{OFF}. \tag{1}$$

where we define the normalized OFF-band counts $C_{OFF} \equiv n \cdot C_{OFF}^{raw}$ with C_{OFF}^{raw} the measured counts. The net flux and EW in the Hα line are then given by:

$$F(H\alpha)_o = 10^{Zp} \frac{C_{NET}}{T\, R_{ON}(H\alpha)} \tag{2}$$

and

$$H\alpha EW_o = \frac{\int R_{ON}(\lambda) d\lambda}{R_{ON}(H\alpha)} \frac{C_{NET}}{n \cdot C_{OFF}^{raw}}\,. \tag{3}$$

where T is the integration time (sec), 10^{Zp} is the ON-band zero point (erg cm^{-2} sec^{-1}) corrected for atmospheric extinction and $R_{ON}(\lambda)$ is the transmissivity of the ON-filter at the wavelength of the redshifted $H\alpha$ line. Finally, since the stellar continuum is estimated using a broad band r filter that includes the Hα line, a non-negligible (~ 10%) correction must be included (see Boselli et al 2002 and Gavazzi et al. 2006):

$$F(H\alpha) = F(H\alpha)_o \times \left(1 + \frac{\int R_{ON}(\lambda) d\lambda}{\int R_{OFF}(\lambda) d\lambda}\right) \tag{4}$$

and

$$H\alpha EW = H\alpha EW_o \times \frac{\left(1 + \frac{\int R_{ON}(\lambda) d\lambda}{\int R_{OFF}(\lambda) d\lambda}\right)}{\left(1 - \frac{H\alpha EW_o}{\int R_{OFF}(\lambda) d\lambda}\right)}\,, \tag{5}$$

where $R_{OFF}(\lambda)$ is the transmissivity of the OFF filter.

4.3. The SFR Calibration

The star formation rate is derived from the observed, integrated Hα flux ($F(H\alpha)$) after the following corrections are applied: i) Galactic extinction, ii) deblending from [NII], iii) internal extinction (Boselli at al. 2009).

i) Corrections for Galactic extinction A are computed using the color excess $E(B-V)$ obtained from the far-IR dust map of Schlegel et al., (1998). For the broad band photometry, we assume $A(R) = 2.3E(B-V)$ and $A(I) = 1.5E(B-V)$ (Cardelli et al, 1989), while for the $H\alpha$ fluxes we use $A(H\alpha) = 0.6A(B) = 2.6E(B-V)$ (Kennicutt et al, 2008, Cardelli et al, 1989).

ii) The correction for [NII] deblending is obtained by fitting the ratio $([NII]/H\alpha)_{ew}$ vs absolute i-band relation. This requires that AGNs (Seyfer+LINERS) are first identified (and disregarded) using the nuclear (3 arcesc) SDSS spectra and the BTP (Baldwin et al. 1981) diagnostic. For doing so the Balmer lines are corrected for underlying absorption by 5 Å for $H\beta$ (Kennicutt, 1992, Gavazzi et al, 2004) and by 1.3 Å for $H\alpha$ (Gavazzi et al, 2011). We define as Seyfert those galaxies that have the ratio of $([NII]/H\alpha)_{ew} > 0.5$ and $([OIII]/H\beta)_{ew} > 3$ and LINERS galaxies that have the ratio of $([NII]/H\alpha)_{ew} > 0.5$ and $([OIII]/H\beta)_{ew} \leq 3$. After excluding both classes of AGNs, we perform a linear fit between the ratio $([NII]/H\alpha)_{ew}$ and the absolute i-band magnitude (see Figure 6), corresponding to a well established mass-metallicity relation (Tremonti et al. 2004). We obtain a reliable fit with $([NII]/H\alpha)_{ew} = -0.854 \times M_i - 1.326$. The corrected flux is:
$F(H\alpha_{MW;DB}) = F(H\alpha_{MW})/(1 + (1.34 \times [NII]/([NII]/H\alpha)_{ew}))$
where the measured $([NII]/H\alpha)_{ew}$ is used when the a drift-scan spectrum is available from GOLDMine, otherwise the ratio is obtained from the fit with M_i.

iii) The correction for internal extinction is performed using A_{Ha} from the Balmer decrement if integrated drift-scan mode spectra are available and $H\alpha$ and $H\beta$ are both detected in emission (see an asterisk in Column 9 of Table B.3).

Alternatively, when integrated drift-scan mode spectra are unavailable one can apply an average correction as function of the B band luminosity as proposed by Lee et al. (2009): $A_{Ha} = 1.971 + 0.323 \times B + 0.0134 \times B^2$ for $B > -14$, otherwise $A_{Ha} = 0.10$. Mind however that such dependence is very poorly defined, thus we prefer to give in Table B.3 both values (with and without the Lee et al. 2009 correction) and let the reader to decide which value to adopt. To obtain such a correction one must first convert SDSS g(AB) magnitudes into Johnson B mag, adopting the relation: $B = g \times 0.983 + 0.692$ mag (taken from GOLDMine). In this case the dust extinction corrected flux becames:
$F(H\alpha_{MW;DB;AA}) = F(H\alpha_{MW;DB}) - (A_{Ha}/ - 2.5)$
Finally we derive the corrected $H\alpha$ luminosity:
$L(H\alpha_{MW;DB;AA}) = F(H\alpha_{MW;DB;AA}) + 48 + \log((3.086^2) \times 4\pi \times D^2)$ where D is the distance in Mpc. The star formation rate: $\log(SFR) = L(H\alpha_{MW;DB;AA}) - 41.1024$ according to Kennicutt (1998).

The results of integral photometry as derived from the present observations are listed in Table B.3 as follows:

- Column 1: AGC designation, from Haynes et al. (2011).
- Columns 2 and 3: R.A. and Dec. (J2000)
- Column 4: equivalent width of Hα + [NII] (in Å) as given in equation (5)
- Column 5: 1σ uncertainty on the Hα + [NII] equivalent width as given in equation (A.8)
- Column 6: log of Hα + [NII] (in erg cm^{-2} s^{-1}) flux as given in equation (4)
- Column 7: log of 1σ uncertainty on the Hα + [NII] flux as given in equation (A.6)
- Column 8: log of SFR obtained in Sect. 4.3, without correction for internal extinction.
- Column 9: log of SFR[10] including the correction for internal extinction using the Balmer decrement when a drift-scan spectrum is available (see *) or as proposed by Lee et al. (2009) in M$_\odot$ yr^{-1}.
- Column 10: sky quality: P = photometric (σ < 5%), T = transparent (5% < σ < 10%)
- Column 11: Atlas figure

We cross correlated our catalogue with the 11 Mpc volume Hα survey by Kennicutt et al. (2008) and we found 5 galaxies in common (see Table 1). In spite of the paucity of the data, the agreement between the two sets of measurements is satisfactory.

An independent check of the calibration of our Hα measurements has been performed on a significant number of detections by comparing the fluxes determined in 3 arcsec nuclear apertures in our Hα images with the flux in the Hα+[NII] lines listed in the SDSS spectral database obtained in 3 arcsec fibres (after removing all measurements not obtained in the nuclear regions). The comparison, given in Figure 7, shows a very satisfactory agreeement between the imaging and the spectral flux determinations.

The final SFRs, plotted against M_i are presented in Figure 8. The error bars are obtained combining in quadrature the errors on $F(H\alpha)$ (see eq. 11) with the error on the coefficient of absorption from the Milky Way. Errors on the extinction coefficient A_{Ha} and on the correction for deblending are not considered (see Boselli et al. 2009). The linear regression is SFR=$-0.39 * M_i - 8.21$, with r=0.87, i.e. in the whole sample the global SFR is proportional to the i band luminosity.

Table 1. Comparison between the photometry from this work and from Kennicutt et al. 2008

AGC	log F(Hα + [NII]) erg cm^{-2} s^{-1}	EW Å	log F$_{\mathrm{Ken}}$ erg cm^{-2} s^{-1}	EW$_{\mathrm{Ken}}$ Å
(1)	(2)	(3)	(4)	(5)
5456	-12.28 ± 0.04	42.33 ± 4.23	-12.32 ± 0.01	46 ± 6
6082	<-12.13 ± 0.00	0.00 ± 3.20	-12.92 ± 0.23	1 ± 1
6272	-11.86 ± 0.16	9.11 ± 3.40	-11.71 ± 0.03	14 ± 1
6328	-11.26 ± 0.14	9.78 ± 3.16	-11.53 ± 0.04	5 ± 1
8091	-12.40 ± 0.04	90.03 ± 10.69	-12.35 ± 0.01	103 ± 9

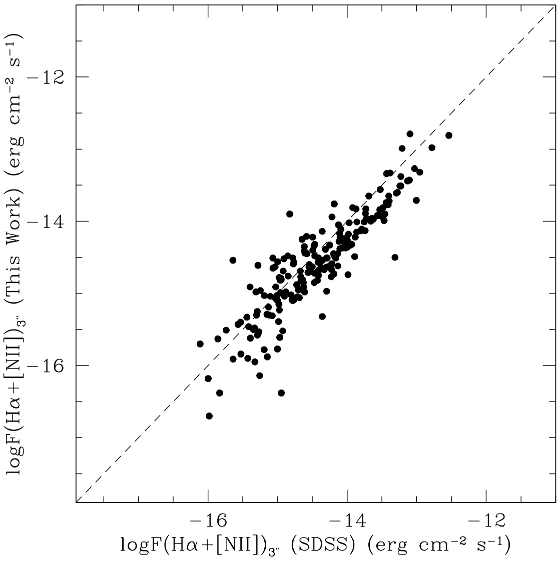

Fig. 7. Comparison between the Hα + [NII] flux extracted in 3 arcsec aperture centered on the nucleus (from this work) and the flux in the Hα + [NII] lines given by SDSS in 3 arcsec fibre spectrum (for detections with SN> 2). The dashed line gives the one-to-one relation.

5. Summary and Future Prospects

This is the first paper of a series devoted to Hα3, the Hα narrow-band imaging survey of galaxies carryed out with the San Pedro Martir 2.1m telescope (Mexico), selected from the HI Arecibo Legacy Fast ALFA Survey (ALFALFA).

The first sample includes ∼ 400 targets in the Local Supercluster for the sky region 11$^{\mathrm{h}}$ < R.A. < 16$^{\mathrm{h}}$; 4$^{\mathrm{o}}$ < Dec. < 16$^{\mathrm{o}}$; 350 < cz < 2000 km s^{-1} including the Virgo cluster.

At the distance of Virgo (17 Mpc) and given the sensitivity of ALFALFA the targets selected for the Hα follow-up contain more than $10^{7.7}$ M$_\odot$ of neutral atomic hydrogen. Hα3, complete for $M_{HI} > 10^8$ M$_\odot$, provides the full census of the star formation in HI rich galaxies of the local universe over a broad range of stellar masses, from dwarf galaxies with $10^{7.5}$ $M_\odot$ up to giants with $10^{11.5}$ $M_\odot$. Not unexpectedly, only an handful number of detections is identified with galaxies on the red sequence, while

---

[10] Among galaxies detected in photometric conditions, SFR is given only for objects strictly belonging to the Hα3 sample, i.e. in the interval 11$^{\mathrm{h}}$ < R.A. < 16$^{\mathrm{h}}$; 4$^{\mathrm{o}}$ < Dec. < 16$^{\mathrm{o}}$; and for 350 < cz < 2000 km s^{-1} (outside Virgo) and 350 < cz < 3000 km s^{-1} (inside Virgo). For few sporadic galaxies observed in spite of not belonging to such interval, we give flux and EW, but we don't convert it into SFR.

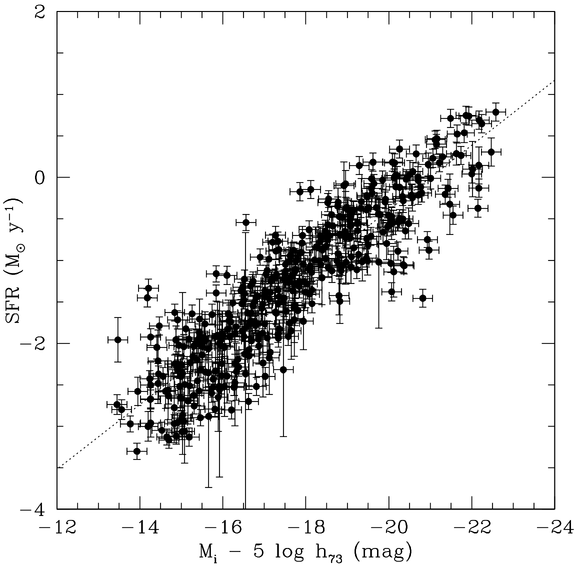

Fig. 8. The corrected SFR derived from this work (see Column 9 of Table B.3) as a function of the absolute i band magnitude M_i .

the majority are late-type, from giant spirals (Sa-Sd) to dwarf Irr-BCDs.

In this paper, we present the properties of the Hα galaxy sample, together with Hα fluxes and equivalent widths for the yet unpublished subsample observed between 2006 and 2009. The integrated Hα fluxes are corrected for galactic and internal extinction and for [NII] contamination providing us with the global star formation rates (SFR). Given the sensitivity of the present Hα observations, we detect galaxies with an unobscured SFR density above $3x10^{-9}$ $M_\odot$ yr^{-1} pc^{-2} at 1σ.

The analysis of the integrated quantities (global SFR) produced by Hα3 will be carryed out in Paper II of this series (Gavazzi et al. 2012). By using hydrogen recombination lines as a tracer of recent star formation, we aim to investigate the relationships between atomic neutral gas and newly formed stars in different environments (cluster and field), morphological types (spirals and dwarfs), and over a wide range of stellar masses ($\sim 10^{7.5} - 10^{11.5}$ $M_\odot$). Paper III will contain the extension of Hα3 to the Coma supercluster ($10^h < \text{R.A.} < 16^h; 24^o < \text{Dec.} < 28^o; 3900 < cz < 9000$ km s^{-1}). Being approximately 6 times more distant than Virgo, galaxies selected by ALFALFA at Coma contain about 35 times more HI than those at Virgo. Hence ALFALFA will be complete for $\geq 10^{9.5}$ $M_\odot$, thus for giant galaxies. The cost of missing completely the population of dwarf galaxies will be compensated by the fact that at $cz > 5000$ the shredding problem affecting the SDSS completeness is much less severe than at Virgo, hence making it possible to extract a catalogue of optically selected candidates from the SDSS database. This will allow us to investigate in details the differences between the optical and the radio selection functions.

Appendix A: The error budget

As mentioned in Sect. 4.1, for extended sources, the dominant source of error in the final Hα fluxes is associated with variations of the background on scales similar to the source, which depend on the quality of the flat-fielding. We measure the background in several regions comparable with the size of the galaxies and we establish that this fluctuation is on average ∼ 10% of the sky rms on the individual pixels. This error is dominant over the Poisson statistical uncertainty on the number counts. Therefore, the total uncertainty on the ON and OFF counts is proportional to the number of pixels N_{pixel} occupied by each galaxy, as derived from the optical major and minor axes, a and b respectively (see Gavazzi et al. 2002a):

$$\sigma_{ON} = 0.1\, rms_{ON}\, N_{pixel} \tag{A.1}$$

$$\sigma_{OFF}^{raw} = 0.1\, rms_{OFF}\, N_{pixel} \tag{A.2}$$

An additional source of error affecting the OFF counts derives from the uncertainty on the normalization coefficient n which we estimate to be ∼ 3%, thus:

$$\sigma_{OFF} = \sqrt{(n \cdot \sigma_{OFF}^{raw})^2 + (0.03\, n \cdot C_{OFF}^{raw})^2}. \tag{A.3}$$

The error on the NET counts is defined as:

$$\sigma_{NET} = \sqrt{(\sigma_{ON})^2 + (\sigma_{OFF})^2}. \tag{A.4}$$

The error on the Hα flux finally becomes:

$$\sigma_{F_o} = \left[\left(\frac{10^{Zp}\sigma_{C_{NET}}}{T R_{ON}(H\alpha)}\right)^2 + \left(0.05 \cdot 10^{Zp} \ln(10)\, F_o\right)^2\right]^{0.5} \tag{A.5}$$

$$\sigma_F = \sigma_{F_o} \times \left(1 + \frac{\int R_{ON}(\lambda)d\lambda}{\int R_{OFF}(\lambda)d\lambda}\right). \tag{A.6}$$

The second term in Eq. (A.5) accounts for the uncertainty on the photometric calibration, which we estimate to be 5%.

Similarly, for the EWs, we compute the final error as:

$$\sigma_{EW_o} = \frac{\int R_{ON}(\lambda)d\lambda}{R_{ON}(H\alpha)} \left[\left(\frac{\sigma_{NET}}{n \cdot C_{OFF}^{raw}}\right)^2 + \left(\frac{C_{NET}\sigma_{OFF}}{(n \cdot C_{OFF}^{raw})^2}\right)^2\right]^{0.5} \tag{A.7}$$

$$\sigma_{EW} = \sigma_{EW_o} \times \frac{\left(1 + \frac{\int R_{ON}(\lambda)d\lambda}{\int R_{OFF}(\lambda)d\lambda}\right)}{\left(1 - \frac{H\alpha EW}{\int R_{OFF}(\lambda)d\lambda}\right)^2}. \tag{A.8}$$

In conclusion this error budget results from several components (photometric accuracy, flat fielding), even if a systematic uncertainty on the normalization factor, as derived from the measurement of foreground stars, is the dominant source of error (Spector et al. 2011).

Appendix B: The Atlas

Images of the OFF and NET frames of galaxies with Hα observations presented in this work are given separately for 102 galaxies with substantial Hα structure in Fig. 9; for 84 marginal detections (<2σ) or with unresolved/complex Hα emission in Fig. 10. For the 47 remaining galaxies with no Hα emission, the OFF-band images are shown in Fig. 11. Galaxies are labeled with their celestial coordinates. A 1 arcmin bar is given.

Acknowledgements. This work is dedicated to the memory of Gaby Garcia who payed with his life the passion for his work. We thank the night operators, specially Felipe Montalvo and Salvador Monrroy for their collaboration, the resident astronomers at SPM for their assistance during the observations and the mexican TAC for the generous time allocation. We acknowledge useful discussions with Luis Aguillar, Luis Carrasco, Matteo Fossati, Michael Richter and Giulia Savorgnan. We thank L. Giordano, D. Burlon, E. Farina, C. Pacifici and V. Presotto for their help during the observations and L. Cortese and S. Zibetti, F. Martinelli and I. Arosio for their support in the data reduction.
The authors would like to acknowledge the work of the entire ALFALFA collaboration team in observing, flagging, and extracting the catalog of galaxies used in this work. This research has made use of the GOLDMine database (Gavazzi G. et al. 2003) and of the NASA/IPAC Extragalactic Database (NED) which is operated by the Jet Propulsion Laboratory, California Institute of Technology, under contract with the National Aeronautics and Space Administration.
Funding for the Sloan Digital Sky Survey (SDSS) and SDSS-II has been provided by the Alfred P. Sloan Foundation, the Participating Institutions, the National Science Foundation, the U.S. Department of Energy, the National Aeronautics and Space Administration, the Japanese Monbukagakusho, and the Max Planck Society, and the Higher Education Funding Council for England. The SDSS Web site is *http://www.sdss.org/*. The SDSS is managed by the Astrophysical Research Consortium (ARC) for the Participating Institutions. The Participating Institutions are the American Museum of Natural History, Astrophysical Institute Potsdam, University of Basel, University of Cambridge, Case Western Reserve University, The University of Chicago, Drexel University, Fermilab, the Institute for Advanced Study, the Japan Participation Group, The Johns Hopkins University, the Joint Institute for Nuclear Astrophysics, the Kavli Institute for Particle Astrophysics and Cosmology, the Korean Scientist Group, the Chinese Academy of Sciences (LAMOST), Los Alamos National Laboratory, the Max-Planck-Institute for Astronomy (MPIA), the Max-Planck-Institute for Astrophysics (MPA), New Mexico State University, Ohio State University, University of Pittsburgh, University of Portsmouth, Princeton University, the United States Naval Observatory, and the University of Washington.
G.G. acknowledges financial support from italian MIUR PRIN contract 200854ECE5. R.G. and M.P.H. are supported by US NSF grants AST-0607007 and AST-1107390 and by a Brinson Foundation grant.

References

Abazajian, K. N., et al. 2009, ApJS, 182, 543
Baldwin, J. A., Phillips, M. M., & Terlevich, R. 1981, PASP, 93, 5
Bell, E. F., McIntosh, D. H., Katz, N., & Weinberg, M. D. 2003, ApJS, 149, 289
Bigiel, F., Leroy, A., Walter, F., Brinks, E., de Blok, W. J. G., Madore, B., & Thornley, M. D. 2008, AJ, 136, 2846
Bigiel, F., Leroy, A., Walter, F., Blitz, L., Brinks, E., de Blok, W. J. G., & Madore, B. 2010, AJ, 140, 1194
Boselli, A., & Gavazzi, G. 2002, A&A, 386, 124
Boselli, A., Iglesias-Páramo, J., Vílchez, J. M., & Gavazzi, G. 2002, A&A, 386, 134
Boselli, A. & Gavazzi, G. 2006, PASP, 118, 517
Boselli, A., Boissier, S., Cortese, L., Buat, V., Hughes, T. M., & Gavazzi, G. 2009, ApJ, 706, 1527
Bothwell, M. S., Kennicutt, R. C., & Lee, J. C. 2009, MNRAS, 400, 154
Cardelli, J. A., Clayton, G. C., & Mathis, J. S. 1989, ApJ, 345, 245
Catinella, B., Schiminovich, D., Kauffmann, G., et al. 2010, MNRAS, 403, 683
Conselice, C. J. 2003, ApJS, 147, 1
Cortese, L., & Hughes, T. M. 2009, MNRAS, 400, 1225
Dreyer, J. L. E. 1888, MmRAS, 49, 1
Dreyer, J. L. E. 1908, MmRAS, 59, 105
Fumagalli, M., & Gavazzi, G. 2008, A&A, 490, 571
Fumagalli, M., Krumholz, M. R., Prochaska, J. X., Gavazzi, G., & Boselli, A. 2009, ApJ, 697, 1811
Fumagalli, M., da Silva, R. L., & Krumholz, M. R. 2011, ApJ, 741, L26
Gavazzi, G., Pierini, D., & Boselli, A. 1996, A&A, 312, 397
Gavazzi, G., Boselli, A., Scodeggio, M., Pierini, D., & Belsole, E. 1999, MNRAS, 304, 595
Gavazzi, G., Boselli, A., Pedotti, P., Gallazzi, A., & Carrasco, L. 2002a, A&A, 386, 114
Gavazzi, G., Boselli, A., Pedotti, P., Gallazzi, A., & Carrasco, L. 2002b, A&A, 396, 449
Gavazzi, G., Boselli, A., Donati, A., Franzetti, P., & Scodeggio, M. 2003, A&A, 400, 451
Gavazzi, G., Zaccardo, A., Sanvito, G., Boselli, A., & Bonfanti, C. 2004, A&A, 417, 499
Gavazzi, G., Boselli, A., Cortese, L., et al. 2006, A&A, 446, 839
Gavazzi, G., Giovanelli, R., Haynes, M. P., et al. 2008, A&A, 482, 43
Gavazzi, G., Fumagalli, M., Cucciati, O., & Boselli, A. 2010, A&A, 517, A73
Gavazzi, G., Savorgnan, G., & Fumagalli, M. 2011, A&A, 534, A31
Gavazzi, G., Fumagalli, M., Galardo, V., Grossetti, F, Boselli, A., Giovanelli, R., Haynes, M. P., Fabello, S., 2012, Paper II, submitted to A&A
Giovanelli, R., Haynes, M. P., Kent, B. R., et al. 2005, AJ, 130, 2598
Giovanelli, R., Haynes, M. P., Kent, B. R., et al. 2007, AJ, 133, 2569
Glover, S. C. O., & Clark, P. C. 2011, arXiv:1105.3073
Haynes, M. P., Giovanelli, R., Salzer, J. J., et al. 1999, AJ, 117, 1668
Haynes, M. P., Giovanelli, R., Martin, A. M., et al. 2011, AJ, 142, 170
Huang, S., Haynes, M.P., Giovanelli, R., Brinchmann, J., Stierwalt, S. and Neff, S.G., 2011a, A.J. (submitted)
Huang, S., Haynes, M.P., Giovanelli, R. and Brinchmann, J., 2011b, A.J.(submitted)
James, P. A., et al. 2004, A&A, 414, 23
Kapferer, W., Sluka, C., Schindler, S., Ferrari, C., & Ziegler, B. 2009, A&A, 499, 87
Kennicutt, R. C., Jr. 1989, ApJ, 344, 685
Kennicutt, R. C., Jr. 1992, ApJ, 388, 310
Kennicutt, R. C., Jr. 1998, ApJ, 498, 541
Kennicutt, R. C., Jr., Calzetti, D., Walter, F., et al. 2007, ApJ, 671, 333
Kennicutt, R. C., Jr., Lee, J. C., Funes, S. J., José G., Sakai, S., & Akiyama, S. 2008, ApJS, 178, 247
Kent, B. R., Giovanelli, R., Haynes, M. P., et al. 2008, AJ, 136, 713
Koopmann, R. A., & Kenney, J. D. P. 2004, ApJ, 613, 851
Kronberger, T., Kapferer, W., Ferrari, C., Unterguggenberger, S., & Schindler, S 2008, A&A, 481, 337
Krumholz, M. R., Leroy, A. K., & McKee, C. F. 2011, ApJ, 731, 25
Lee, J. C., Kennicutt, R. C., Funes, S. J., José G., Sakai, S., & Akiyama, S. 2007, ApJ, 671, L113
Lee, J. C., Gil de Paz, A., Tremonti, C., et al. 2009, ApJ, 706, 599
Martin, A. M., Papastergis, E., Giovanelli, R., et al. 2010, ApJ, 723, 1359
Mei, S., Blakeslee, J. P., Côté, P., et al. 2007, ApJ, 655, 144
Meurer, G. R., Hanish, D. J., Ferguson, H. C., et al. 2006, ApJS, 165, 307
Meurer, G. R., Wong, O. I., Kim, J. H., et al. 2009, ApJ, 695, 765
Meyer, M. J., Zwaan, M. A., Webster, R. L., et al. 2004, MNRAS, 350, 1195
Nilson, P. 1973, Acta Universitatis Upsaliensis. Nova Acta Regiae Societatis Scientiarum Upsaliensis - Uppsala Astronomiska Observatoriums Annaler, Uppsala: Astronomiska Observatorium, 1973,
Pflamm-Altenburg, J., Weidner, C., & Kroupa, P. 2007, ApJ, 671, 1550
Rose, J. A., Robertson, P., Miner, J., & Levy, L. 2010, AJ, 139, 765
Saintonge, A. 2007, AJ, 133, 2087
Schlegel, D. J., Finkbeiner, D. P., & Davis, M. 1998, ApJ, 500, 525
Schmidt, M. 1959, ApJ, 129, 243
Schruba, A., et al. 2011, arXiv:1105.4605
Spector, O., Finkelman, I., & Brosch, N. 2012, MNRAS, 419, 2156
Tonnesen, S., & Bryan, G. L. 2009, ApJ, 694, 789
Tremonti, C. A., Heckman, T. M., Kauffmann, G., et al. 2004, ApJ, 613, 898
Vogt, N. P., Haynes, M. P., Giovanelli, R., & Herter, T. 2004, AJ, 127, 3300
Vollmer, B., Braine, J., Pappalardo, C., & Hily-Blant, P. 2008, A&A, 491, 455
Vollmer, B., Soida, M., Chung, A., Chemin, L., Braine, J., Boselli, A., & Beck, R. 2009, A&A, 496, 669
von der Linden, A., Wild, V., Kauffmann, G., White, S. D. M., & Weinmann, S. 2010, MNRAS, 404, 1231
Weisz, D. R., Dalcanton, J. J., Williams, B. F., et al. 2011, ApJ, 739, 5
Welikala, N., Connolly, A. J., Hopkins, A. M., Scranton, R., & Conti, A. 2008, ApJ, 677, 970
Wong, T., & Blitz, L. 2002, ApJ, 569, 157
Zwicky, F., Herzog, E., & Wild, P. 1968, Pasadena: California Institute of Technology (CIT), 1961-1968,

Table B.1. Basic data for the 235 target galaxies

AGC (1)	*R.A.* (*J*2000) hhmmss.s (2)	*DEC* $^{o}\ '\ ''$ (3)	CGCG (4)	UGC (5)	NGC (6)	IC (7)	Ty (8)	*cz* km s^{-1} (9)	*a* arcmin (10)	*b* arcmin (11)	*i* mag (12)	*g* mag (13)	*Dist* Mpc (14)
4880	091517.0	115308	62010	4880	-	530	Sab	4971	1.8	0.6	12.6	13.8	66.5
190160	091647.8	112709	62015	-	-	-	-	4954	0.5	0.1	13.7	13.8	66.7
202488	100610.8	110602	-	-	-	-	-	2505	0.1	0.1	15.5	16.0	32.7
5456	100719.7	102143	64068	5456	-	-	Sm	537	1.6	0.8	13.1	13.5	5.9
5741	103442.8	111148	65059	5741	3279	622	Scd	1383	2.0	0.5	12.2	13.4	17.7
208399	104010.7	045432	-	-	-	-	-	747	0.5	0.3	15.7	16.9	20.0
202024	104457.5	115458	-	-	-	-	dS0	869	0.3	0.1	17.2	17.6	10.6
6077	110002.4	145028	95085	6077	3485	-	Sb	1432	1.8	1.5	11.6	12.4	24.5
6082	110018.6	135404	66084	6082	3489	-	S0a	695	2.8	0.8	9.8	10.9	14.1
202040	110301.9	080254	-	-	-	-	S..	1359	0.7	0.5	17.0	17.6	24.5
210023	110426.4	114521	66109	-	-	-	Im	777	1.0	0.5	15.3	15.8	18.3
6167	110656.8	071026	38129	6167	3531	-	Sc	1416	1.9	0.4	12.9	13.6	24.5
6169	110703.4	120334	66115	6169	-	-	Sb	1551	1.7	0.4	13.2	14.0	26.2
210082	110923.2	105003	67014	-	-	-	Im	1555	0.8	0.8	14.3	15.0	25.0
6209	110955.9	104312	67019	6209	3547	-	Sb	1584	1.6	0.8	12.5	13.1	26.6
210111	111025.1	100734	67022	-	-	-	Sdm	1320	0.7	0.5	15.3	15.7	22.8
213064	111054.5	093719	-	-	-	-	S..	1604	0.6	0.4	14.8	15.2	26.5
6233	111128.3	065426	39056	6233	-	-	S0a	1605	1.1	0.4	13.6	14.5	26.5
6245	111239.8	090321	67032	6245	-	676	S0	1421	1.7	1.0	12.0	13.1	24.9
6248	111251.7	101200	-	6248	-	-	Im	1286	0.7	0.7	15.2	15.7	22.6
212097	111300.1	075143	-	-	-	-	Sc	1396	1.2	0.4	14.2	15.0	23.7
219197	111355.2	040619	-	-	-	-	Im/BCD	1609	0.6	0.6	15.7	16.2	20.0
6272	111437.0	124902	67040	6272	3593	-	S0a	631	4.9	2.0	10.2	11.4	13.4
6277	111506.2	144712	96013	6277	3596	-	Sc	1193	3.7	3.5	10.9	11.7	21.2
212132	111626.3	042011	39094	-	-	-	Scd	1104	1.0	0.3	14.6	15.5	20.3
215241	111702.7	100836	-	-	-	-	S..	1765	0.5	0.2	17.2	17.7	20.0
6305	111730.0	043319	39103	6305	3611	-	Sa	1612	2.5	1.7	11.7	12.6	26.8
6328	111855.7	130532	67054	6328	3623	-	Sa	803	6.7	1.9	8.5	9.7	15.9
202257	111914.4	115707	-	-	-	-	Im	860	0.5	0.3	16.2	16.6	17.1
213074	111928.1	093544	-	-	-	-	Im/BCD	990	0.4	0.2	16.2	16.7	18.6
6350	112016.9	133513	67058	6350	3628	-	Sb	844	13.4	2.4	8.9	9.9	16.4
6387	112218.6	130354	67064	6387	-	2763	S0a	1572	1.3	0.4	14.3	14.8	26.4
211370	112223.2	130440	-	-	-	2767	S..	1083	0.6	0.2	16.4	16.8	19.6
213512	112250.7	122041	-	-	-	2781	Im/BCD	1544	0.4	0.3	16.2	16.6	26.2
6420	112426.2	112030	67071	6420	3666	-	Sc	1059	2.5	1.0	11.5	12.4	19.4
215142	112444.5	151632	-	-	-	-	Sdm	1125	0.6	0.2	16.0	16.5	20.3
214317	112505.4	040716	-	-	-	-	S..	1619	0.5	0.2	16.9	17.2	27.0
6438	112553.5	095913	67073	6438	-	692	S..	1156	0.8	0.5	13.6	14.3	20.8
210340	112711.0	084353	67078	-	-	2828	Im/BCD	1046	0.7	0.5	14.2	14.7	19.2
6474	112824.0	092426	67084	6474	3692	-	Sb	1716	3.5	0.7	11.7	12.8	28.7
213939	112824.3	060704	-	-	-	-	Im	1571	0.5	0.2	16.8	17.2	26.4
6498	113007.6	091636	67093	6498	3705	-	Sab	1019	4.9	2.0	10.4	11.4	18.9
215304	113201.9	143639	-	-	-	-	S0a	1124	0.9	0.2	15.4	16.2	19.7
215306	113350.1	144928	-	-	-	-	Im/BCD	1129	0.4	0.2	16.1	16.7	18.0
210459	113419.3	131918	68004	-	-	2934	Sb	1195	0.8	0.4	14.8	15.2	21.3
212838	113453.4	110110	-	-	-	-	Im	881	0.9	0.6	17.7	18.2	17.0
213155	113708.8	131504	-	-	-	-	Sdm	983	0.6	0.2	16.8	17.1	18.3
6605	113813.0	120643	68014	6605	3773	-	S0	983	1.2	1.0	12.7	13.4	18.4
6626	113952.9	085229	68018	6626	-	718	Im	1984	1.2	0.7	13.5	14.1	32.2
6633	114018.6	090035	68021	6633	-	719	S0	1810	1.6	0.6	12.3	13.5	30.5
215137	114056.6	140429	-	-	-	-	S0a	909	0.8	0.3	15.4	16.0	17.7
6644	114058.8	112816	68024	6644	3810	-	Sc	992	3.6	2.7	10.2	10.9	18.5
6655	114150.5	155824	97059	6655	-	-	S0	750	1.3	0.5	13.9	14.5	14.9
6669	114218.1	145941	-	6669	-	-	Im	1019	1.7	0.6	15.2	15.6	18.8
212839	114310.4	141325	-	-	-	-	Im	1017	1.1	0.4	17.1	17.7	18.7
213333	114327.0	112354	-	-	-	-	Im/BCD	897	0.4	0.2	15.8	16.2	17.5
213338	114443.5	111226	-	-	-	-	Im	2956	0.4	0.3	16.5	16.8	45.6
6717	114445.8	091245	-	6717	-	-	Im	2869	1.2	1.0	14.9	15.4	18.0
6730	114526.7	090938	68055	6730	3876	-	Sab	2892	1.2	0.8	13.0	13.4	44.9
6747	114624.1	134938	68063	6747	-	-	Sd	2696	0.9	0.1	16.0	15.7	42.0
210822	115002.7	150124	97159	-	-	-	BCD	756	0.6	0.4	15.0	15.0	20.0
210835	115056.0	143541	97163	-	-	-	S..	1009	0.6	0.3	14.9	15.1	18.6
210861	115201.8	135243	68079	-	-	-	Sd	967	0.7	0.6	15.4	15.7	18.4
213385	115748.1	120224	-	-	-	-	Im	2761	0.9	0.3	15.4	16.0	43.0
210968	115933.8	135315	69010	-	-	-	Sm	1448	1.0	0.7	14.3	14.6	24.7
7001	120110.4	140614	69024	7001	4019	755	Sb	1509	2.6	0.4	13.4	13.7	18.0
7003	120121.5	142659	-	7003	-	-	Im	1287	0.6	0.3	16.3	16.8	22.3
7002	120123.8	132401	69027	7002	4037	-	Sb	930	3.0	2.6	11.9	12.7	18.0
211006	120127.5	140204	69029	-	-	-	BCD	1479	0.7	0.6	14.1	14.6	25.0
211013	120144.2	054917	41023	-	-	-	Sb	1350	0.7	0.5	14.2	14.7	23.5
225078	120302.8	063005	-	-	-	-	Im/BCD	1318	0.4	0.4	15.9	16.4	22.6
224235	120315.1	100628	-	-	-	-	S..	2547	0.7	0.2	16.1	16.6	39.7

Continued in next page

Continued from previous page

AGC (1)	*R.A.* (*J*2000) hhmmss.s (2)	*DEC* ° ′ ″ (3)	CGCG (4)	UGC (5)	NGC (6)	IC (7)	Ty (8)	*cz* km s^{-1} (9)	*a* arcmin (10)	*b* arcmin (11)	*i* mag (12)	*g* mag (13)	*Dist* Mpc (14)
7038	120350.6	143303	-	-	-	-	Im	891	0.8	0.5	16.7	16.4	16.9
224236	120404.4	044847	-	-	-	-	Sdm	2227	0.6	0.2	16.2	16.4	35.7
7048	120411.6	105115	69036	7048	4067	-	Sb	2415	1.2	1.0	12.2	13.0	17.0
224237	120447.1	103735	69043	7066	4078	-	S..	2572	1.3	0.5	16.5	17.0	17.0
220133	120831.1	150548	-	-	-	-	Im	587	0.5	0.4	16.1	17.2	12.7
224602	121003.3	114249	-	-	-	-	Sd	2557	0.9	0.3	16.4	16.9	40.5
220168	121024.2	131014	-	-	-	-	BCD	1699	0.3	0.2	15.5	16.1	32.0
220171	121035.7	114538	69070	-	-	-	BCD	1296	1.0	0.4	14.8	15.5	32.0
224696	121038.0	130119	-	-	-	-	Im	2394	0.3	0.2	17.1	17.1	38.0
220172	121040.8	143846	-	-	-	-	Im	2466	0.4	0.3	17.6	18.0	32.0
224807	121309.4	133504	-	-	-	-	S/BCD	2100	0.4	0.2	17.1	17.5	33.7
7233	121350.3	071203	41049	7233	4191	-	S0a	2659	1.7	1.1	12.2	13.3	32.0
220217	121402.2	064323	41050	-	-	-	Sa	2433	1.0	0.4	14.1	15.2	32.0
224487	121412.1	124658	-	-	-	-	S..	613	0.4	0.2	16.4	17.0	13.2
224244	121413.6	085430	-	-	-	-	Sdm	1933	0.4	0.1	17.1	17.2	32.3
224245	121428.2	055431	-	-	-	-	S..	1921	0.6	0.2	16.2	16.6	31.6
224094	121432.8	120611	-	-	-	-	-	2115	0.4	0.3	16.9	17.3	32.0
220231	121435.7	091159	-	-	-	-	Im	1787	0.6	0.4	16.0	16.3	32.0
224249	121527.4	103044	-	-	-	-	Im/BCD	1990	0.4	0.2	16.9	17.5	25.3
220257	121553.7	140130	-	-	-	-	Im	683	0.4	0.4	16.4	16.9	17.0
224250	121627.0	060307	-	-	-	-	Sm/BCD	2029	0.3	0.2	17.7	17.9	32.7
224251	121634.0	101222	-	-	-	-	Im/BCD	2072	0.1	0.1	17.2	17.5	33.6
221988	121727.8	071936	-	-	-	-	S..	2056	0.5	0.2	16.4	16.7	33.3
224489	121728.1	125556	-	-	-	-	Sc	2202	0.5	0.1	16.2	16.9	20.0
223407	121843.8	122308	-	-	-	-	dE	132	0.8	0.7	15.9	16.8	17.0
220351	121911.0	125301	-	-	-	-	Im	2188	1.0	0.4	15.7	16.2	17.0
227894	121920.1	062432	-	-	-	-	S..	1969	0.4	0.1	17.6	18.8	20.0
7365	121930.6	145238	99014	7365	4262	-	S0	1367	1.9	1.6	10.8	11.9	17.0
220383	121953.4	063956	-	-	-	-	Im	480	0.9	0.6	15.7	16.6	32.0
7376	121949.4	052749	42026	7376	4270	-	S0	2377	2.2	1.0	11.5	12.6	23.0
7380	121956.2	052038	42028	7380	4273	-	Sc	2379	2.0	1.3	11.4	12.1	32.0
220419	122100.1	124333	-	-	-	-	Im	672	0.4	0.4	16.3	16.8	17.0
7445	122238.5	114802	70034	7445	4313	-	Sab	1442	5.1	1.2	11.0	12.1	17.0
220478	122307.4	134440	-	-	-	-	Im	1888	0.6	0.4	16.5	16.8	17.0
227958	122318.4	053626	-	-	-	-	S..	1787	0.5	0.1	16.0	16.6	20.0
225022	122405.1	081738	-	-	-	-	Im/BCD	1370	0.3	0.2	16.7	16.8	23.8
220561	122601.4	081135	-	-	-	-	Im	1304	0.3	0.3	17.4	18.3	17.0
220594	122655.7	095256	-	-	-	-	Im	981	0.8	0.4	16.7	16.8	23.0
226357	122712.8	073821	-	-	-	-	S/BCD	1179	0.4	0.2	17.6	17.7	20.0
223724	122933.6	131146	-	-	-	-	dE	1215	0.3	0.1	17.6	18.0	17.0
7742	123450.8	153304	99093	7742	4540	-	Scd	1288	2.6	1.9	11.4	12.3	17.0
220815	123513.8	102554	-	-	-	-	Sd	1072	1.0	0.1	16.3	17.0	17.0
225847	123856.9	133306	-	-	-	-	Im	982	0.3	0.2	17.8	17.7	18.0
224009	124119.3	063123	-	-	-	-	-	1721	0.6	0.2	16.2	16.7	17.0
227896	124420.9	060522	-	-	-	-	Sdm	1289	0.3	0.1	16.1	16.8	17.0
7920	124445.4	122101	-	7920	-	-	S..	849	2.6	0.8	12.9	13.7	16.1
227970	124601.4	042252	-	-	-	-	Im/BCD	642	0.5	0.2	16.7	16.9	17.0
7943	124645.6	055719	43023	7943	-	-	Scd	837	2.2	1.8	12.9	13.6	16.0
222216	124759.5	042558	43029	-	-	-	Im	1038	1.0	0.6	14.7	15.2	18.9
7976	124915.8	043921	43035	7976	-	-	Pec	2666	1.0	1.0	14.6	15.1	41.4
224304	124925.7	042333	-	-	-	-	Sdm	2642	0.6	0.4	15.6	16.2	41.2
224226	124959.3	054915	-	-	-	-	Im/BCD	624	0.5	0.5	15.9	16.6	13.3
225857	125059.5	090439	-	-	-	-	S/BCD	1115	0.5	0.2	16.1	16.6	18.0
223205	125106.8	120336	-	-	-	-	Im	1787	0.3	0.2	16.4	16.9	29.0
221085	125258.8	142357	-	-	-	-	Im	1040	0.7	0.3	16.3	16.7	18.3
225850	125402.1	092649	-	-	-	-	S..	1815	0.4	0.1	16.6	17.1	18.0
8032	125444.2	131414	71071	8032	-	-	S..	1121	2.7	0.7	12.7	13.7	19.6
224902	125446.3	153530	-	-	-	-	Im/BCD	2651	0.3	0.3	16.1	16.5	40.7
8042	125510.3	075503	43065	8042	-	-	Sc	2661	1.3	0.8	14.4	15.2	41.1
8045	125523.5	075434	43068	8045	-	-	Im	2798	0.9	0.7	13.6	14.4	43.2
8053	125549.0	040050	43070	8053	-	-	Sd	708	1.3	0.5	14.1	14.5	14.2
8056	125619.9	101118	71075	8056	-	-	Sd	2697	1.4	0.7	14.3	14.7	41.8
8061	125644.0	115555	-	-	-	-	Im	563	0.9	0.9	15.3	15.9	12.0
222259	125653.3	080940	43078	-	-	-	S..	2596	0.7	0.2	15.3	15.9	40.3
222260	125657.0	040353	43077	-	-	-	Sdm	828	1.0	0.5	14.3	14.9	15.8
8085	125817.3	143323	100018	8085	-	-	Scd	2041	2.6	0.6	13.2	13.9	32.5
8091	125840.4	141302	71087	8091	-	-	Im	213	1.1	1.0	14.0	14.5	7.2
221245	125852.8	130910	71090	-	-	-	Im	1910	0.9	0.6	14.4	15.0	30.5
8102	125927.0	141014	71092	8102	4866	-	Sa	1984	5.3	1.0	10.5	11.7	31.7
225851	125942.6	110438	-	-	-	-	S/BCD	2792	0.5	0.3	15.6	16.2	18.0
8114	130025.0	134013	71095	8114	-	-	Sc	1990	1.1	0.5	15.0	15.2	31.7
8166	130352.4	105820	71102	8166	-	-	Scd	2943	1.0	0.1	15.4	16.2	45.0
230077	130623.3	102600	71109	-	-	-	Im	930	0.6	0.4	15.0	15.4	17.1

Continued in next page

Continued from previous page

AGC (1)	*R.A.* (*J2000*) hhmmss.s (2)	*DEC* ° ′ ″ (3)	CGCG (4)	UGC (5)	NGC (6)	IC (7)	Ty (8)	*cz* km s^{-1} (9)	*a* arcmin (10)	*b* arcmin (11)	*i* mag (12)	*g* mag (13)	*Dist* Mpc (14)
230084	130655.9	144826	101001	-	-	-	Im	984	0.4	0.3	15.3	15.9	18.0
8276	131206.3	052832	-	8276	-	-	Im	913	0.6	0.3	15.8	16.2	16.9
8285	131233.3	071103	44026	8285	-	-	Im	898	1.7	0.4	14.0	14.6	16.6
8298	131319.7	101137	72026	8298	-	-	Im	1157	1.3	1.0	14.2	14.7	20.1
8345	131652.1	123254	72042	8345	5058	-	S..	966	0.8	0.8	13.6	14.0	17.3
233627	131953.0	134823	-	-	-	-	Im	937	0.4	0.1	16.8	17.2	18.0
8382	132032.2	052426	44072	8382	-	-	Im	966	1.0	0.6	14.3	14.9	17.5
8385	132038.1	094714	72049	8385	-	-	Sdm	1133	1.8	0.9	13.3	13.8	19.7
8450	132701.2	100322	72076	8450	-	-	Im	1049	0.8	0.6	14.7	15.2	18.5
230436	133438.0	084737	73036	-	-	-	Im	1231	0.8	0.6	14.5	14.9	20.9
8575	133545.5	085806	73044	8575	-	-	Im	1163	2.6	0.4	14.2	14.7	20.0
231022	133602.6	081105	-	-	-	-	Sdm	1245	1.2	0.1	15.9	16.3	21.1
232025	133643.6	083247	73051	-	-	-	Im	1166	0.7	0.4	15.2	15.8	19.7
8616	133732.1	085306	73054	8616	5248	-	Sbc	1151	5.7	4.6	9.7	10.6	19.8
8629	133830.6	082632	73056	8629	-	-	Im	1021	0.8	0.3	15.2	15.7	17.9
233601	133850.8	080629	-	-	-	-	Im	1188	0.2	0.1	17.1	17.6	20.0
238771	134641.0	063915	-	-	-	-	S..	1293	0.4	0.2	15.5	16.3	20.0
8800	135326.5	051227	45132	8800	5338	-	S0	824	2.3	1.0	13.1	14.0	15.0
8821	135411.2	051336	45137	8821	5348	-	Sbc	1450	3.5	0.5	12.6	13.5	23.8
8831	135458.4	052000	46001	8831	5356	-	Sbc	1367	3.7	0.8	11.8	13.0	22.7
232141	135504.5	051122	-	-	-	-	Im	1398	0.4	0.4	16.4	16.8	23.1
232142	135609.4	053233	-	-	-	-	Im	1096	0.7	0.4	16.4	17.0	18.6
8853	135612.0	050052	46009	8853	5364	-	Sbc	1240	6.8	4.4	10.0	10.9	20.8
233571	135741.0	152224	-	-	-	-	Sdm	1249	0.4	0.2	15.9	16.2	18.0
233718	135843.4	141541	-	-	-	-	Im/BCD	1277	0.3	0.2	16.3	16.8	18.0
8995	140447.3	084802	74083	8995	-	-	Sm	1235	2.1	1.1	13.5	14.1	20.6
9020	140631.8	060145	46050	9020	5470	-	Sb	1021	1.5	0.6	12.4	13.7	17.7
243852	140704.5	104245	-	-	-	-	S..	1178	0.5	0.2	16.7	17.2	20.0
243881	141750.7	065023	-	-	-	-	Im	1248	0.3	0.1	16.4	16.8	20.0
9169	141944.7	092144	75008	9169	-	-	Sm	1283	5.1	0.7	13.2	13.9	20.8
714055	142044.5	083735	-	-	-	-	Im	1300	0.8	0.3	15.7	16.4	21.2
9202	142210.7	135503	75020	9202	5587	-	S0a	2303	2.3	0.7	12.2	13.2	35.0
9225	142424.3	081632	75027	9225	-	-	Sm	1260	1.0	0.5	14.7	15.3	20.5
9249	142659.8	084100	75033	9249	-	-	Sm	1365	2.2	0.4	14.1	14.6	22.0
9252	142710.8	050806	47042	9252	-	-	Im	1585	1.0	0.2	15.3	15.8	25.3
9273	142810.9	133305	75042	9273	-	-	Im	1287	1.0	0.5	14.3	14.8	20.8
9275	142818.5	134648	75045	9275	-	1014	Sdm	1287	2.4	1.4	12.5	13.1	20.8
244386	142852.8	123454	-	-	-	-	BCD	1974	0.2	0.1	17.0	17.6	18.0
9328	143039.6	071629	47070	9328	5645	-	Sm	1367	2.6	1.0	11.8	12.5	22.0
716018	143048.7	070925	-	-	-	-	S..	1356	0.2	0.1	17.3	17.8	20.0
240441	143220.7	095600	75063	-	-	-	Im/BCD	1369	0.6	0.5	14.5	15.3	22.3
9353	143243.8	095329	75064	9353	5669	-	Scd	1367	4.0	2.8	11.5	12.1	22.0
9363	143324.3	042700	47090	9363	5668	-	Sd	1583	3.3	3.0	11.3	11.9	25.0
9380	143438.8	041537	47104	9380	-	-	Im	1682	1.9	1.0	14.4	15.1	26.5
9385	143522.8	051636	-	9385	-	-	Im	1636	0.5	0.4	14.6	15.2	25.7
9389	143533.2	125427	75082	9389	-	-	Sb	1823	2.3	0.6	13.5	13.9	28.1
9394	143539.9	131012	75084	9394	-	-	Im	1799	2.0	0.4	13.9	14.4	27.8
240523	143640.9	113437	75090	-	-	-	Sb	1767	2.5	0.6	15.4	16.0	27.7
9436	143911.0	052147	47127	9436	5701	-	S0	1505	4.3	4.1	10.4	11.6	23.8
714204	143912.4	090805	-	-	-	-	S/BCD	1759	0.5	0.2	15.5	16.0	20.0
249303	144119.2	074735	-	-	-	-	S..	1766	0.6	0.4	15.7	16.1	27.4
9483	144257.9	045324	48004	9483	-	1048	S..	1633	2.2	0.7	12.2	13.3	25.5
9485	144302.8	044554	48007	9485	-	-	S..	1699	1.4	0.4	14.8	15.3	26.5
242618	144329.2	043153	-	-	-	-	Im	1716	0.6	0.5	15.5	16.0	27.0
9500	144521.4	075145	-	9500	-	-	Im	1690	2.8	2.8	14.4	15.0	26.2
242016	144624.3	141247	-	-	-	-	Im	1789	1.4	0.9	16.2	16.6	25.1
240700	144728.4	124553	76047	-	-	-	Im/BCD	1825	0.5	0.3	15.3	15.6	27.6
9535	144842.5	122724	76063	9535	5762	-	Sa	1794	1.3	1.3	12.7	13.5	27.5
245076	145243.5	114020	-	-	-	-	S..	1803	0.8	0.3	16.4	16.9	23.9
241727	145837.8	064630	48085	-	-	-	Im/BCD	1673	0.4	0.3	15.1	15.6	25.8
257898	152059.4	121052	-	-	-	-	Sdm	1161	0.4	0.2	16.3	16.6	18.0
9824	152156.5	050412	49146	9824	5921	-	Sbc	1480	4.9	4.0	10.8	11.8	22.7
9830	152300.8	043145	49152	9830	-	-	Sc	1830	1.9	0.2	14.3	15.3	27.5
258405	152411.4	072918	-	-	-	-	S..	1815	1.0	0.3	15.1	16.3	20.0
9845	152605.4	091216	77127	9845	-	-	Scd	1893	1.5	0.2	14.4	15.4	28.3
252085	153139.0	153532	-	-	-	-	Im	1767	0.8	0.8	15.2	15.6	2.5
9895	153343.1	150025	107003	9895	5951	-	Sc	1777	3.5	0.8	12.4	13.2	26.4
9902	153433.1	150759	-	9902	-	-	Scd	1694	1.0	0.3	16.6	17.0	25.2
257920	153446.6	122650	-	-	-	-	Im/BCD	2687	0.3	0.2	16.1	16.6	18.0
9908	153458.6	114500	78017	9908	5956	-	Sc	1901	1.5	1.5	12.2	13.1	28.0
257921	153507.9	122013	-	-	-	-	Im	1842	0.7	0.3	16.3	16.9	20.0
9915	153523.2	120250	78018	9915	5957	-	Sb	1828	2.7	2.7	11.6	12.6	27.1
9935	153736.2	055825	50047	9935	5964	4551	Sd	1446	4.2	3.2	11.5	12.4	21.9

Continued in next page

Continued from previous page

AGC (1)	*R.A.* (*J*2000) hhmmss.s (2)	*DEC* o ′ ″ (3)	CGCG (4)	UGC (5)	NGC (6)	IC (7)	Ty (8)	*cz* km s^{-1} (9)	*a* arcmin (10)	*b* arcmin (11)	*i* mag (12)	*g* mag (13)	*Dist* Mpc (14)
9941	153821.9	125738	78033	9941	-	-	Im	1861	1.6	1.5	15.0	15.8	27.4
9943	153830.0	121110	78034	9943	5970	-	Sc	1955	2.9	1.9	11.0	11.9	28.8
257927	153836.7	133103	-	-	-	-	S..	2404	-	-	-	-	-
257929	153857.5	123256	-	-	-	-	Im/BCD	1773	0.5	0.4	15.5	16.2	18.0
9987	154253.0	141354	78052	9987	5984	-	Scd	1105	2.9	0.8	12.2	13.1	16.9
9991	154323.9	142608	107029	9991	-	-	Sc	1935	1.8	0.5	13.9	14.7	28.3
10014	154544.0	123038	78063	10014	-	-	Im	1124	0.9	0.7	14.8	15.5	17.1
10023	154609.8	065353	50100	10023	-	-	Im	1405	1.1	0.5	14.7	15.3	21.1
10083	155413.8	143603	107054	10083	6012	-	Sab	1854	2.7	2.6	11.7	12.6	27.0
252891	155636.8	061139	-	-	-	-	Im	1933	0.7	0.4	16.1	16.7	28.0
258430	155955.5	065303	-	-	-	-	S..	1558	0.4	0.1	17.0	17.7	20.0
261969	160602.2	083025	79046	-	-	-	Im	1369	0.8	0.3	15.4	16.0	20.1
261313	160641.0	063451	51043	-	-	-	Im/BCD	1755	0.6	0.5	14.6	15.2	25.7
10219	160817.0	073216	51052	10219	-	1197	Sd	1370	3.0	0.5	13.2	14.1	20.1
268216	161220.5	063237	-	-	-	-	Im	1723	0.5	0.4	17.1	17.3	20.0
214319+	112607.8	040345	-	-	-	-	Im/BCD	1417	0.3	0.2	17.1	17.6	19.2
213169+	113517.3	045725	-	-	-	-	Im/BCD	1525	0.4	0.3	16.2	16.7	17.7

Concluded from previous page

Table B.2. $H\alpha$ observational specifications of the 235 target galaxies

		ON					OFF			
AGC (1)	Date yymmdd (2)	T_{exp} sec (3)	N_{exp} (4)	A.M. (5)	Zp erg cm^{-2} s^{-1} (6)	Seeing arcsec (7)	T_{exp} sec (8)	N_{exp} (9)	Seeing arcsec (10)	n (11)
4880	2006-05-01	900	1	1.10	-15.52	1.6	180	1	1.8	0.376
190160	2006-05-01	900	1	1.14	-15.52	2.0	180	1	1.7	0.464
202488	2006-04-26	900	1	1.21	-15.51	1.8	180	1	1.8	0.486
5456	2006-04-24	900	1	1.07	-15.51	1.8	180	1	1.5	0.460
5741	2006-04-23	900	1	1.07	-15.51	2.2	180	1	1.9	0.460
208399	2008-04-12	1200	3	1.13	-15.45	1.6	300	3	1.5	0.358
202024	2006-04-25	900	3	1.08	-15.51	2.0	240	3	2.0	0.386
6077	2007-04-19	900	1	1.12	-15.45	1.6	180	1	1.6	0.470
6082	2009-04-29	300	3	1.06	-15.40	1.8	180	1	1.5	0.200
202040	2008-04-11	1200	1	1.18	-15.45	2.1	240	1	2.0	0.458
210023	2009-04-27	420	3	1.08	-15.40	1.7	240	1	1.4	0.177
6167	2008-04-09	900	1	1.36	-15.45	2.3	180	1	2.2	0.458
6169	2007-04-20	900	1	1.15	-15.45	1.9	180	1	1.7	0.460
210082	2009-04-27	300	3	1.06	-15.40	1.6	180	1	1.6	0.168
6209	2006-04-30	900	1	1.07	-15.51	1.7	180	1	1.6	0.458
210111	2009-04-28	300	3	1.10	-15.40	1.9	240	2	1.8	0.105
213064	2009-04-28	300	3	1.08	-15.40	1.9	180	1	1.6	0.164
6233	2008-04-08	900	1	1.10	-15.45	1.5	180	1	1.4	0.420
6245	2008-04-08	900	1	1.36	-15.45	1.8	180	1	1.6	0.458
6248	2009-04-27	420	5	1.07	-15.40	1.9	240	1	1.4	0.175
212097	2008-04-09	900	1	1.27	-15.45	2.1	180	1	2.0	0.458
219197	2009-04-30	300	3	1.12	-15.40	1.7	180	1	1.8	0.121
6272	2007-04-19	900	1	1.12	-15.45	1.6	180	1	1.6	0.470
6277	2006-04-24	900	1	1.04	-15.51	1.8	180	1	1.4	0.480
212132	2008-04-11	900	1	1.19	-15.45	1.9	180	1	1.7	0.482
215241	2009-04-29	420	3	1.08	-15.40	1.9	240	1	1.6	0.173
6305	2008-04-08	900	1	1.27	-15.45	1.5	180	1	1.3	0.458
6328	2007-04-20	600	1	1.10	-15.45	1.8	60	1	1.7	0.880
202257	2007-04-23	600	3	1.05	-15.45	1.9	240	1	1.9	0.240
213074	2008-04-08	1200	1	1.09	-15.45	1.4	240	1	1.4	0.482
6350	2007-04-19	600	1	1.10	-15.45	1.4	180	1	1.4	0.310
6387	2007-04-22	900	1	1.19	-15.45	1.6	240	1	1.5	0.350
211370	2007-04-22	900	1	1.19	-15.45	1.6	240	1	1.6	0.350
213512	2007-04-23	900	1	1.15	-15.45	1.9	180	2	1.9	0.480
6420	2006-05-01	900	1	1.06	-15.51	1.8	180	1	1.4	0.473
215142	2007-04-24	600	6	1.08	-15.45	2.0	240	4	2.1	0.180
214317	2008-04-11	1200	1	1.17	-15.45	1.7	240	1	1.6	0.482
6438	2008-04-10	900	1	1.08	-15.45	2.2	180	1	1.6	0.458
210340	2008-04-09	900	1	1.24	-15.45	2.0	180	1	1.9	0.482
6474	2008-04-09	900	1	1.17	-15.45	1.8	180	1	1.9	0.458
213939	2009-04-29	420	3	1.10	-15.40	1.6	180	3	1.3	0.257
6498	2008-04-11	900	1	1.09	-15.45	1.7	180	1	2.1	0.443
215304	2008-04-10	900	1	1.04	-15.45	1.7	180	1	1.6	0.482
215306	2007-04-26	900	1	1.05	-15.45	1.6	180	1	1.5	0.490
210459	2008-04-08	1200	1	1.11	-15.45	1.5	240	1	1.4	0.482
212838	2009-04-28	600	3	1.07	-15.40	1.9	240	2	1.5	0.262
213155	2006-04-29	600	3	1.05	-15.51	2.3	240	1	2.3	0.224
6605	2007-04-22	900	1	1.15	-15.45	1.7	180	1	1.7	0.450
6626	2007-04-20	900	1	1.12	-15.45	1.7	180	1	1.7	0.460
6633	2007-04-22	600	1	1.09	-15.45	1.5	180	1	1.5	0.300
215137	2006-04-25	600	3	1.06	-15.51	2.0	240	1	1.6	0.238
6644	2007-04-19	900	1	1.06	-15.45	1.6	180	1	1.5	0.460
6655	2007-04-22	900	1	1.10	-15.45	1.6	180	1	1.6	0.480
6669	2007-04-20	600	3	1.05	-15.45	1.7	240	1	1.8	0.240
212839	2009-04-27	300	6	1.07	-15.40	2.2	240	2	1.4	0.124
213333	2007-04-26	900	1	1.06	-15.45	1.6	180	1	1.5	0.510
213338	2007-04-24	600	3	1.09	-15.45	1.8	240	1	1.9	0.240
6717	2007-04-24	600	7	1.08	-15.45	1.6	240	2	1.6	0.220
6730	2007-04-22	900	1	1.09	-15.45	1.5	180	1	1.4	0.480
6747	2007-04-23	900	1	1.05	-15.45	1.9	180	1	2.1	0.460
210822	2008-04-08	1200	1	1.06	-15.45	1.6	240	1	1.4	0.482
210835	2007-04-23	900	1	1.04	-15.45	1.7	180	1	1.7	0.510
210861	2006-04-24	600	3	1.05	-15.51	1.6	180	2	1.6	0.305
213385	2007-04-23	900	1	1.13	-15.45	1.7	180	1	1.7	0.380
210968	2006-04-23	900	1	1.06	-15.51	2.0	180	1	2.0	0.440
7001	2007-04-23	900	1	1.05	-15.45	1.6	180	1	1.9	0.460
7003	2008-04-13	1200	1	1.42	-15.45	1.6	240	1	1.5	0.446
7002	2007-04-20	900	1	1.05	-15.45	1.5	180	1	1.7	0.470
211006	2008-04-14	420	3	1.05	-15.45	1.6	240	2	1.4	0.174
211013	2008-04-09	900	1	1.23	-15.45	1.9	180	1	1.9	0.458
225078	2009-04-28	300	3	1.09	-15.40	1.7	180	1	1.5	0.157

Continued in next page

Continued from previous page

		ON					OFF			
AGC	Date	T_{exp}	N_{exp}	A.M.	Zp	Seeing	T_{exp}	N_{exp}	Seeing	n
	yymmdd	sec			erg cm^{-2} s^{-1}	arcsec	sec		arcsec	
(1)	(2)	(3)	(4)	(5)	(6)	(7)	(8)	(9)	(10)	(11)
224235	2007-04-26	900	1	1.07	-15.45	1.4	180	1	1.4	0.470
7038	2008-04-08	1200	1	1.05	-15.45	1.4	240	1	1.4	0.458
224236	2008-04-09	1200	1	1.19	-15.45	1.8	240	1	1.9	0.482
7048	2007-04-20	900	1	1.07	-15.45	1.6	180	1	1.8	0.420
224237	2007-04-22	600	3	1.10	-15.45	1.4	240	1	1.4	0.230
220133	2009-04-29	420	3	1.04	-15.40	1.7	240	1	1.2	0.192
224602	2006-05-01	600	2	1.12	-15.51	1.9	240	1	1.6	0.197
220168	2008-04-09	1200	1	1.07	-15.45	1.8	240	1	1.6	0.435
220171	2007-04-23	900	1	1.17	-15.45	1.8	180	1	1.7	0.490
224696	2007-04-19	600	3	1.13	-15.45	1.6	240	1	1.4	0.220
220172	2009-04-28	600	3	1.04	-15.40	1.4	180	3	1.1	0.389
224807	2006-04-30	600	3	1.05	-15.51	1.6	240	1	1.6	0.234
7233	2008-04-13	900	1	1.11	-15.45	1.5	180	1	1.3	0.458
220217	2009-04-30	300	3	1.10	-15.40	2.0	180	1	1.4	0.156
224487	2007-04-20	600	3	1.06	-15.45	1.4	240	1	1.4	0.240
224244	2007-04-25	600	4	1.10	-15.45	1.6	240	1	1.9	0.270
224245	2009-04-30	300	3	1.10	-15.40	1.9	180	1	1.9	0.168
224094	2007-04-20	600	3	1.20	-15.45	1.4	240	1	1.5	0.210
220231	2006-04-29	600	3	1.17	-15.51	2.2	240	1	1.7	0.199
224249	2006-04-29	900	1	1.10	-15.51	2.4	180	1	2.1	0.374
220257	2006-04-25	780	5	1.05	-15.45	1.6	240	4	1.6	0.430
224250	2008-04-09	1200	1	1.15	-15.45	1.8	240	1	1.7	0.458
224251	2007-04-26	900	1	1.09	-15.45	1.3	180	1	1.4	0.460
224489	2006-04-30	900	1	1.09	-15.51	1.6	180	1	1.4	0.453
221988	2008-04-12	900	1	1.09	-15.45	1.6	180	1	1.6	0.458
223407	2007-04-19	600	3	1.35	-15.45	2.4	240	1	1.6	0.230
220351	2006-04-26	600	3	1.06	-15.51	1.7	240	1	1.6	0.263
227894	2008-04-11	1200	1	1.19	-15.45	1.7	240	1	1.8	0.458
7365	2007-04-19	600	1	1.05	-15.45	1.4	30	1	1.4	1.800
220383	2008-04-09	1200	2	1.19	-15.45	2.2	240	2	2.3	0.458
7376	2008-04-13	900	1	1.15	-15.45	1.6	180	1	1.3	0.458
7380	2006-04-22	600	2	1.15	-15.51	2.0	240	1	1.8	0.280
220419	2006-04-25	660	4	1.40	-15.51	2.1	600	4	1.5	0.087
7445	2007-04-19	900	1	1.06	-15.45	1.6	180	1	1.6	0.440
220478	2007-04-23	600	3	1.17	-15.45	1.8	240	1	1.6	0.250
227958	2009-04-30	300	3	1.10	-15.40	1.9	180	1	1.7	0.167
225022	2007-04-24	900	3	1.10	-15.45	1.8	180	3	1.6	0.400
220561	2008-04-08	1200	1	1.09	-15.45	1.4	240	1	1.4	0.458
220594	2007-04-24	600	4	1.28	-15.45	2.2	240	1	1.9	0.240
226357	2008-04-10	1200	1	1.09	-15.45	2.2	240	1	2.0	0.482
223724	2007-04-22	600	6	1.18	-15.45	1.5	240	2	1.6	0.240
7742	2006-04-23	900	1	1.06	-15.51	2.5	180	1	2.3	0.404
220815	2008-04-10	1200	1	1.07	-15.45	1.8	240	1	1.9	0.458
225847	2007-04-25	600	4	1.10	-15.45	1.7	240	2	1.6	0.220
224009	2006-04-26	600	3	1.20	-15.51	1.9	240	1	1.4	0.200
227896	2008-04-08	1200	1	1.10	-15.45	1.3	240	1	1.4	0.458
7920	2006-04-23	900	1	1.06	-15.51	2.0	180	1	2.0	0.460
227970	2008-04-11	1200	1	1.21	-15.45	1.8	240	1	2.1	0.482
7943	2009-04-28	300	3	1.10	-15.40	1.1	180	1	1.3	0.173
222216	2009-04-30	300	3	1.12	-15.40	1.6	180	1	2.0	0.191
7976	2008-04-08	900	1	1.12	-15.45	1.2	180	1	1.2	0.470
224304	2008-04-13	1200	1	1.47	-15.45	1.8	240	1	1.7	0.446
224226	2009-04-30	300	3	1.12	-15.40	1.3	180	1	1.1	0.169
225857	2007-04-27	600	4	1.09	-15.45	1.9	240	3	1.9	0.220
223205	2009-04-27	300	5	1.07	-15.40	1.5	240	2	1.2	0.108
221085	2006-04-26	600	3	1.39	-15.51	1.8	240	1	1.5	0.222
225850	2008-04-11	1200	1	1.12	-15.45	1.7	240	1	1.6	0.446
8032	2006-04-23	900	1	1.08	-15.51	1.8	180	1	1.7	0.440
224902	2007-04-20	900	1	1.33	-15.45	1.6	180	1	1.6	0.450
8042	2009-04-28	420	3	1.09	-15.40	1.4	240	1	1.6	0.169
8045	2008-04-09	900	1	1.09	-15.45	1.8	180	1	1.8	0.470
8053	2008-04-13	1200	2	1.21	-15.45	1.8	240	2	1.8	0.446
8056	2007-04-22	900	1	1.38	-15.45	2.3	180	1	1.8	0.460
8061	2006-04-24	600	3	1.15	-15.51	1.4	240	1	1.3	0.230
222259	2007-04-24	900	1	1.09	-15.45	2.1	180	1	2.9	0.470
222260	2008-04-08	900	1	1.14	-15.45	1.1	180	1	1.3	0.458
8085	2007-04-20	900	1	1.45	-15.45	1.5	180	1	1.6	0.460
8091	2008-04-08	900	1	1.09	-15.45	1.1	180	1	1.2	0.458
221245	2007-04-23	900	1	1.25	-15.45	1.9	180	1	2.1	0.480
8102	2006-04-22	900	1	1.31	-15.51	2.2	180	1	2.5	0.463
225851	2007-04-26	900	1	1.07	-15.45	1.4	180	1	1.5	0.460
8114	2007-04-20	900	1	1.62	-15.45	1.5	180	1	1.5	0.450

Continued in next page

Continued from previous page

		ON					OFF			
AGC (1)	Date yymmdd (2)	T_{exp} sec (3)	N_{exp} (4)	A.M. (5)	Zp erg cm^{-2} s^{-1} (6)	Seeing arcsec (7)	T_{exp} sec (8)	N_{exp} (9)	Seeing arcsec (10)	n (11)
8166	2007-04-26	900	1	1.15	-15.45	1.5	180	1	1.5	0.450
230077	2007-04-26	600	3	1.10	-15.45	1.3	240	1	1.6	0.230
230084	2007-04-24	900	1	1.07	-15.45	1.9	180	1	1.9	0.470
8276	2008-04-13	1200	1	1.49	-15.45	1.8	240	2	1.5	0.458
8285	2008-04-09	900	1	1.19	-15.45	2.3	180	1	1.9	0.458
8298	2007-04-23	600	4	1.30	-15.45	2.1	240	2	2.1	0.280
8345	2007-04-19	900	1	1.40	-15.45	1.9	180	1	1.6	0.460
233627	2007-04-27	600	4	1.07	-15.45	1.8	240	3	1.9	0.240
8382	2008-04-10	1200	1	1.16	-15.45	1.6	240	1	1.9	0.458
8385	2007-04-19	900	1	1.50	-15.45	1.5	180	1	1.5	0.450
8450	2007-04-24	600	3	1.27	-15.45	1.8	240	1	2.2	0.260
230436	2007-04-24	900	1	1.60	-15.45	2.2	180	1	2.3	0.450
8575	2007-04-20	900	1	1.50	-15.45	1.4	180	1	1.7	0.420
231022	2008-04-10	1200	1	1.15	-15.45	1.8	240	1	1.7	0.458
232025	2007-04-22	600	3	1.40	-15.45	3.0	240	1	2.0	0.230
8616	2007-04-19	600	1	1.59	-15.45	2.0	180	1	1.8	0.300
8629	2007-04-26	900	1	1.16	-15.45	1.4	180	1	1.3	0.460
233601	2009-04-29	600	3	1.11	-15.40	1.4	180	3	1.1	0.360
238771	2008-04-09	1200	1	1.19	-15.45	1.7	240	1	1.9	0.458
8800	2009-04-30	300	3	1.11	-15.40	1.6	180	1	2.0	0.178
8821	2008-04-13	900	1	1.24	-15.45	1.7	180	1	1.6	0.458
8831	2008-04-07	900	1	1.13	-15.45	2.0	180	1	1.5	0.458
232141	2009-04-28	420	3	1.11	-15.40	1.5	240	1	1.2	0.171
232142	2009-04-26	420	3	1.10	-15.40	1.6	180	1	1.8	0.262
8853	2006-04-25	900	1	1.29	-15.51	1.7	180	1	1.4	0.460
233571	2007-04-26	600	3	1.19	-15.45	1.4	240	1	1.5	0.250
233718	2007-04-26	600	3	1.30	-15.45	1.4	240	1	1.6	0.250
8995	2008-04-08	900	1	1.09	-15.45	1.3	180	1	1.3	0.458
9020	2008-04-13	900	1	1.11	-15.45	1.3	180	1	1.2	0.458
243852	2009-04-30	300	3	1.07	-15.40	2.0	180	1	1.9	0.162
243881	2008-04-13	1200	1	1.31	-15.45	1.6	240	1	1.2	0.482
9169	2008-04-08	900	1	1.13	-15.45	1.4	180	1	1.3	0.458
714055	2008-04-09	900	1	1.11	-15.45	2.4	180	1	2.3	0.482
9202	2007-04-19	900	1	1.40	-15.45	1.8	180	1	1.4	0.430
9225	2008-04-10	1200	2	1.12	-15.45	1.6	240	1	1.4	0.482
9249	2009-04-26	300	3	1.08	-15.40	1.6	180	1	2.0	0.167
9252	2008-04-10	1200	1	1.20	-15.45	1.6	240	1	1.4	0.458
9273	2007-04-19	900	1	1.48	-15.45	1.8	180	1	1.7	0.470
9275	2007-04-18	900	1	1.23	-15.45	1.4	180	1	1.5	0.260
244386	2007-04-20	900	1	1.32	-15.45	1.5	180	1	1.6	0.450
9328	2006-04-24	900	1	1.25	-15.51	1.9	180	1	1.3	0.472
716018	2008-04-11	1200	1	1.13	-15.45	1.6	240	1	1.5	0.458
240441	2008-04-09	900	1	1.11	-15.45	2.2	180	1	2.4	0.458
9353	2006-04-24	900	1	1.28	-15.51	2.1	180	1	1.4	0.485
9363	2008-04-07	900	1	1.17	-15.45	2.2	180	1	1.5	0.443
9380	2008-04-08	1200	1	1.20	-15.45	1.4	240	1	1.4	0.458
9385	2008-04-10	1200	1	1.28	-15.45	1.6	240	1	1.7	0.443
9389	2007-04-18	900	1	1.30	-15.45	1.5	180	1	1.6	0.480
9394	2007-04-18	900	1	1.42	-15.45	1.5	180	1	1.5	0.460
240523	2009-04-28	420	3	1.08	-15.40	1.2	240	1	1.6	0.175
9436	2008-04-11	900	1	1.34	-15.45	1.9	180	1	1.7	0.458
714204	2008-04-11	1200	1	1.14	-15.45	1.5	240	1	1.4	0.458
249303	2009-04-29	300	3	1.09	-15.40	1.6	240	1	1.2	0.112
9483	2006-04-29	900	1	1.29	-15.51	2.3	180	1	2.0	0.461
9485	2008-04-11	1200	1	1.12	-15.45	1.6	240	1	1.6	0.458
242618	2008-04-11	1200	1	1.12	-15.45	1.6	240	1	1.6	0.435
9500	2008-04-11	1200	1	1.10	-15.45	1.6	240	1	1.5	0.458
242016	2009-04-29	600	3	1.06	-15.40	1.6	180	3	1.4	0.397
240700	2007-04-20	900	1	1.40	-15.45	1.5	180	1	1.7	0.440
9535	2006-04-26	900	1	1.13	-15.51	1.7	180	1	1.4	0.461
245076	2009-04-26	300	4	1.06	-15.40	1.8	180	1	1.5	0.163
241727	2008-04-11	1200	1	1.17	-15.45	1.6	240	1	1.4	0.435
257898	2007-04-22	900	1	1.14	-15.45	2.0	180	1	1.7	0.470
9824	2008-04-07	900	1	1.24	-15.45	1.7	180	1	1.7	0.458
9830	2008-04-07	900	1	1.14	-15.45	1.6	180	1	1.5	0.458
258405	2008-04-08	900	1	1.15	-15.45	1.4	180	2	1.6	0.435
9845	2008-04-07	900	1	1.12	-15.45	1.6	180	1	1.4	0.482
252085	2009-04-28	300	3	1.06	-15.40	1.1	240	1	1.2	0.099
9895	2009-04-28	300	3	1.04	-15.40	1.2	180	1	1.7	0.209
9902	2009-04-30	600	3	1.05	-15.40	2.3	180	3	1.1	0.392
257920	2007-04-22	600	3	1.20	-15.45	2.0	240	1	1.8	0.220
9908	2009-04-28	300	3	1.07	-15.40	1.5	180	1	1.9	0.106

Continued in next page

Continued from previous page

		ON					OFF			
AGC	Date	T_{exp}	N_{exp}	A.M.	Zp	Seeing	T_{exp}	N_{exp}	Seeing	n
	yymmdd	sec			erg cm^{-2} s^{-1}	arcsec	sec		arcsec	
(1)	(2)	(3)	(4)	(5)	(6)	(7)	(8)	(9)	(10)	(11)
257921	2009-04-26	420	3	1.05	-15.40	2.1	240	1	1.8	0.187
9915	2007-04-18	900	1	1.28	-15.45	1.6	180	1	1.5	0.410
9935	2008-04-07	900	1	1.22	-15.45	1.7	180	1	1.7	0.458
9941	2009-04-26	420	4	1.07	-15.40	2.0	240	1	1.3	0.173
9943	2006-04-22	900	1	1.06	-15.51	2.1	180	1	1.6	0.450
257927	2007-04-26	600	3	1.15	-15.45	1.6	240	1	1.6	0.220
257929	2007-04-26	720	3	1.30	-15.45	1.6	180	2	1.7	0.320
9987	2009-04-28	300	3	1.04	-15.40	1.6	180	1	1.3	0.159
9991	2009-04-28	300	4	1.04	-15.40	1.4	180	1	1.1	0.099
10014	2007-04-26	720	3	1.30	-15.45	1.8	180	2	1.6	0.320
10023	2008-04-15	600	3	1.18	-15.45	1.5	100	3	1.3	0.537
10083	2009-04-29	300	3	1.04	-15.40	1.3	603	1	1.1	0.560
252891	2009-04-26	420	3	1.10	-15.40	2.0	240	1	1.7	0.169
258430	2008-04-13	600	3	1.14	-15.45	1.3	240	1	1.3	0.227
261969	2008-04-12	180	5	1.11	-15.45	2.2	180	1	2.1	0.092
261313	2008-04-11	1200	1	1.16	-15.45	1.5	240	1	1.5	0.458
U010219	2008-04-10	900	1	1.19	-15.45	1.9	180	1	1.9	0.458
268216	2008-04-14	600	3	1.14	-15.45	1.4	300	2	1.4	0.188
214319+	2010-04-16	600	3	1.13	-15.80	2.0	240	1	2.0	-
213169+	2010-04-16	600	3	1.11	-15.80	2.0	240	1	2.0	-

Concluded from previous page

Table B.3. Integrated *Hα* photometric parameters of the 235 target galaxies

AGC (1)	*R.A.* (*J*2000) hhmmss (2)	*DEC* ° ′ ″ (3)	HαEW Å (4)	$\sigma_{\rm EW}$ Å (5)	log F(Hα) erg cm^{-2} s^{-1} (6)	log $\sigma_{\rm F}$ erg cm^{-2} s^{-1} (7)	log SFR M$_\odot$ y^{-1} (8)	log SFR M$_\odot$ y^{-1} (9)	Quality (10)	Fig. (11)
4880	091517.0	115308	15.93	3.43	-12.65	0.09	-	-	P	9
190160	091647.8	112709	29.31	3.54	-13.41	0.05	-	-	P	9
202488	100610.8	110602	33.73	4.01	-13.36	0.05	-	-	P	10
5456	100719.7	102143	42.33	3.62	-12.28	0.03	-	-	P	9
5741	103442.8	111148	16.60	3.20	-12.44	0.08	-	-	P	9
208399	104010.7	045432	0.00	3.89	< -14.42	-	-	-	P	11
202024	104457.5	115458	0.00	6.24	< -14.64	-	-	-	P	11
6077	110002.4	145028	16.99	4.08	-12.14	0.10	-0.56	-0.28	P	9
6082	110018.6	135404	0.00	3.20	< -12.13	-	< -1.05	< -0.75	P	11
202040	110301.9	080254	0.00	26.74	< -14.13	-	< -2.34	< -2.30	P	11
210023	110426.4	114521	23.67	16.16	-13.47	0.29	-1.98	-1.92	P	10
6167	110656.8	071026	31.22	4.08	-12.42	0.05	-0.78	-0.59	P	9
6169	110703.4	120334	11.50	3.29	-12.99	0.12	-1.30	-1.13	P	9
210082	110923.2	105003	26.31	9.12	-13.00	0.15	-1.30	-1.18	P	9
6209	110955.9	104312	39.39	3.56	-12.11	0.04	-0.43	-0.19	P	9
210111	111025.1	100734	44.60	18.35	-13.27	0.17	-1.60	-1.52	P	9
213064	111054.5	093719	70.39	7.06	-12.77	0.04	-1.00	-0.89	P	9
6233	111128.3	065426	47.19	3.94	-12.57	0.03	-0.83	-0.67	P	9
6245	111239.8	090321	18.89	4.21	-12.30	0.09	-0.69	-0.46	P	10
6248	111251.7	101200	0.00	48.80	< -13.36	-	< -1.71	< -1.63	P	11
212097	111300.1	075143	26.93	4.87	-13.01	0.07	-1.33	-1.22	P	9
219197	111355.2	040619	28.13	19.96	-13.58	0.30	-1.97	-1.92	P	10
6272	111437.0	124902	9.11	3.37	-11.86	0.16	-0.81	-0.55	P	9
6277	111506.2	144712	22.93	4.47	-11.75	0.08	-0.30	0.00	P	9
212132	111626.3	042011	4.62	4.32	-13.89	0.40	-2.32	-2.24	P	10
215241	111702.7	100836	25.49	15.76	-14.14	0.26	-2.54	-2.50	P	10
6305	111730.0	043319	29.72	4.10	-11.98	0.06	-0.29	-0.02	P	9
6328	111855.7	130532	9.78	3.12	-11.26	0.14	-0.11	0.31	P	9
202257	111914.4	115707	28.97	7.39	-13.75	0.11	-2.29	-2.25	P	10
213074	111928.1	093544	51.39	4.77	-13.40	0.04	-1.87	-1.83	P	9
6350	112016.9	133513	7.73	3.67	-11.45	0.20	-0.26	0.14	P	10
6387	112218.6	130354	17.95	3.49	-13.13	0.08	-1.39	-1.25	P	9
211370	112223.2	130440	0.00	4.23	< -14.53	-	< -2.94	< -2.90	P	11
213512	112250.7	122041	3.63	3.34	-14.54	0.40	-2.71	-2.65	P	10
6420	112426.2	112030	27.42	3.37	-11.91	0.05	-0.50	-0.26	P	9
215142	112444.5	151632	16.79	4.01	-13.81	0.10	-2.18	-2.14	P	10
214317	112505.4	040716	21.38	7.67	-14.09	0.15	-2.20	-2.16	P	9
6438	112553.5	095913	18.02	3.82	-12.94	0.09	-1.39	-1.26	P	9
210340	112711.0	084353	93.80	5.43	-12.41	0.02	-0.89	-0.78	P	9
6474	112824.0	092426	18.08	3.47	-12.21	0.08	-0.48	-0.21	P	9
213939	112824.3	060704	30.11	12.86	-13.93	0.18	-2.07	-2.03	P	10
6498	113007.6	091636	17.10	3.44	-11.68	0.08	-0.32	-0.01	P	9
215304	113201.9	143639	5.64	4.56	-14.15	0.35	-2.57	-2.52	P	10
215306	113350.1	144928	0.00	3.03	< -14.66	-	< -3.16	< -3.10	P	11
210459	113419.3	131918	26.04	3.76	-13.15	0.06	-1.53	-1.44	P	9
212838	113453.4	110110	83.65	52.92	-13.46	0.25	-2.00	-1.96	P	10
213155	113708.8	131504	41.90	4.39	-13.97	0.04	-2.44	-2.40	P	9
6605	113813.0	120643	63.63	4.00	-12.02	0.02	-0.62	-0.45	P	9
6626	113952.9	085229	8.41	3.28	-13.18	0.17	-1.28	-1.08	P	9
6633	114018.6	090035	11.87	3.11	-12.59	0.11	-0.78	-0.54	P	9
215137	114056.6	140429	-0.21	4.12	< -14.34	-	< -2.84	< -2.79	P	11
6644	114058.8	112816	37.25	3.55	-11.23	0.04	0.11	0.45	P	9
6655	114150.5	155824	29.12	3.42	-12.77	0.05	-1.49	-1.40	P	9
6669	114218.1	145941	38.58	12.14	-13.24	0.13	-1.71	-1.64	P	10
212839	114310.4	141325	0.00	36.50	< -14.03	-	< -2.47	< -2.43	P	11
213333	114327.0	112354	-0.22	3.13	< -14.44	-	< -2.94	< -2.90	P	11
213338	114443.5	111226	22.83	3.53	-13.82	0.06	-	-	P	9
6717	114445.8	091245	15.70	9.27	-13.31	0.25	-	-	P	10
6730	114526.7	090938	23.98	3.58	-12.48	0.06	-	-	P	9
6747	114624.1	134938	7.00	4.18	-14.18	0.26	-	-	P	10
210822	115002.7	150124	292.38	13.69	-12.21	0.01	-0.64	-0.54	P	9
210835	115056.0	143541	52.58	3.67	-12.94	0.03	-1.41	-1.33	P	9
210861	115201.8	135243	23.65	4.12	-13.53	0.07	-2.02	-1.95	P	9
213385	115748.1	120224	0.00	4.83	< -14.32	-	-	-	P	11
210968	115933.8	135315	18.59	3.23	-13.20	0.07	-1.50	-1.37	P	9
7001	120110.4	140614	42.66	3.67	-12.47	0.03	-1.06	-0.91	P	9
7003	120121.5	142659	0.00	10.34	< -14.07	-	< -2.36	< -2.32	P	11
7002	120123.8	132401	10.54	5.19	-12.58	0.21	-1.22	-1.02	P	9
211006	120127.5	140204	48.35	4.65	-12.63	0.04	-0.93	-0.79	P	9
211013	120144.2	054917	54.05	4.24	-12.64	0.03	-1.01	-0.88	P	9
225078	120302.8	063005	21.53	10.38	-13.74	0.20	-2.06	-2.00	P	10
224235	120315.1	100628	9.90	3.84	-14.18	0.17	-	-	P	10

Continued in next page

Continued from previous page

AGC (1)	*R.A.* (*J*2000) hhmmss (2)	*DEC* ° ′ ″ (3)	HαEW Å (4)	$\sigma_{\rm EW}$ Å (5)	log F(Hα) erg cm^{-2} s^{-1} (6)	log $\sigma_{\rm F}$ erg cm^{-2} s^{-1} (7)	log SFR M$_\odot$ y^{-1} (8)	log SFR M$_\odot$ y^{-1} (9)	Quality (10)	Fig. (11)
7038	120350.6	143303	16.11	13.65	-13.72	0.36	-2.25	-2.21	P	10
224236	120404.4	044847	20.91	6.06	-13.75	0.12	-	-	P	10
7048	120411.6	105115	22.16	3.42	-12.30	0.06	-1.07	-0.39*	P	9
224237	120447.1	103735	54.92	13.41	-13.59	0.10	-	-	P	10
220133	120831.1	150548	36.21	18.79	-13.74	0.22	-2.52	-2.48	P	10
224602	121003.3	114249	-0.68	3.96	< -14.95	-	< -2.78	< -2.70	P	11
220168	121024.2	131014	9.63	4.10	-13.98	0.18	-2.03	-1.93	P	10
220171	121035.7	114538	5.71	3.08	-13.89	0.23	-1.94	-1.54*	P	10
224696	121038.0	130119	133.57	6.36	-13.39	0.01	-1.23	-1.16	P	10
220172	121040.8	143846	0.30	14.91	< -14.38	-	< -2.36	< -2.32	P	11
224807	121309.4	133504	29.91	4.58	-14.08	0.06	-2.02	-1.97	P	9
7233	121350.3	071203	0.00	3.24	< -13.13	-	< -1.85	< -1.76	P	11
220217	121402.2	064323	16.16	11.79	-13.23	0.31	-1.35	-1.21	P	10
224487	121412.1	124658	10.04	3.56	-14.29	0.15	-3.04	-3.00	P	10
224244	121413.6	085430	28.75	4.84	-14.01	0.07	-2.00	-1.95	P	10
224245	121428.2	055431	0.00	19.61	< -13.91	-	< -1.95	< -1.88	P	11
224094	121432.8	120611	10.82	4.87	-14.41	0.19	-2.40	-2.35	P	10
220231	121435.7	091159	20.22	6.23	-13.86	0.13	-1.90	-1.82	P	10
224249	121527.4	103044	3.97	3.40	-14.91	0.37	-3.10	-3.06	P	11
220257	121553.7	140130	0.00	3.91	< -14.68	-	< -3.21	< -3.17	P	11
224250	121627.0	060307	39.60	13.32	-14.02	0.14	-2.00	-1.96	P	9
224251	121634.0	101222	24.30	3.54	-14.11	0.06	-2.06	-2.01	P	10
221988	121727.8	071936	32.97	4.76	-13.82	0.06	-2.79	-2.75	P	9
224489	121728.1	125556	0.00	7.30	< -14.41	-	< -1.81	< -1.74	P	11
223407	121843.8	122308	0.00	8.50	< -14.14	-	< -2.67	< -2.63	P	11
220351	121911.0	125301	8.89	6.86	-14.09	0.33	-2.61	-2.57	P	10
227894	121920.1	062432	0.00	7.28	< -14.94	-	< -3.34	< -3.30	P	11
7365	121930.6	145238	0.00	3.06	< -12.62	-	< -1.34	< -0.64*	P	11
220383	121953.4	063956	0.00	39.16	< -13.97	-	< -2.03	< -1.95	P	11
7376	121949.4	052749	0.00	3.34	< -12.83	-	< -1.30	< -1.05	P	11
7380	121956.2	052038	44.48	3.83	-11.53	0.03	0.12	0.47	P	9
220419	122100.1	124333	0.00	3.26	< -14.64	-	< -3.16	< -3.12	P	11
7445	122238.5	114802	4.63	3.06	-12.50	0.29	-1.37	-1.14	P	10
220478	122307.4	134440	0.00	11.28	< -14.16	-	< -2.67	< -2.63	P	11
227958	122318.4	053626	30.87	12.82	0.00	-	-	-	T	9
225022	122405.1	081738	12.60	4.00	-14.31	0.14	-2.56	-2.51	P	10
220561	122601.4	081135	0.00	20.84	< -14.47	-	< -3.01	< -2.97	P	11
220594	122655.7	095256	6.85	4.21	-14.46	0.26	-2.74	-2.69	P	10
226357	122712.8	073821	28.56	9.76	-14.22	0.14	-2.62	-2.58	P	10
223724	122933.6	131146	26.39	4.56	-14.30	0.07	-2.84	-2.80	P	10
7742	123450.8	153304	7.66	3.12	-12.45	0.18	-1.15	-0.45*	P	9
220815	123513.8	102554	10.67	10.20	-14.28	0.41	-2.82	-2.78	P	11
225847	123856.9	133306	26.25	4.55	-14.30	0.07	-2.78	-2.74	P	10
224009	124119.3	063123	35.93	6.73	-13.78	0.08	-2.32	-2.28	P	9
227896	124420.9	060522	0.00	5.83	< -14.44	-	< -2.98	< -2.94	P	11
7920	124445.4	122101	-0.61	3.16	< -13.41	-	< -2.10	< -1.41*	P	11
227970	124601.4	042252	68.20	17.88	-13.55	0.10	-2.09	-2.05	P	10
7943	124645.6	055719	25.16	10.13	-12.51	0.17	-1.21	-1.07	P	9
222216	124759.5	042558	19.96	9.21	0.00	-	-	-	T	9
7976	124915.8	043921	40.20	8.98	-12.94	0.09	-0.82	-0.65	P	9
224304	124925.7	042333	14.40	12.22	-13.77	0.36	-1.62	-1.50	P	10
224226	124959.3	054915	22.43	17.94	-13.86	0.34	-2.61	-2.57	P	10
225857	125059.5	090439	74.00	7.82	-13.50	0.04	-1.99	-1.95	P	10
223205	125106.8	120336	50.67	47.85	-13.88	0.39	-1.96	-1.90	P	11
221085	125258.8	142357	22.89	6.95	-14.23	0.13	-2.70	-2.66	P	10
225850	125402.1	092649	0.00	4.80	< -14.68	-	< -3.17	< -3.13	P	11
8032	125444.2	131414	6.55	3.14	-13.04	0.21	-1.58	-1.43	P	9
224902	125446.3	153530	35.26	4.00	-13.59	0.05	-	-	P	10
8042	125510.3	075503	36.74	16.16	-13.00	0.18	-	-	P	9
8045	125523.5	075434	15.43	5.07	-13.08	0.14	-	-	P	9
8053	125549.0	040050	48.18	5.35	-12.63	0.04	-1.37	-1.28	P	10
8056	125619.9	101118	14.16	5.54	-13.22	0.17	-	-	P	9
8061	125644.0	115555	16.43	6.32	-13.70	0.16	-2.54	-2.50	P	10
222259	125653.3	080940	10.96	3.76	-13.79	0.15	-1.67	-1.55	P	9
222260	125657.0	040353	24.61	4.17	-13.07	0.07	-1.72	-1.64	P	9
8085	125817.3	143323	4.31	3.58	-13.37	0.36	-	-	P	10
8091	125840.4	141302	90.05	9.51	-12.40	0.04	-1.68	-1.64	P	9
221245	125852.8	130910	12.18	4.46	-13.40	0.16	-1.53	-1.38	P	9
8102	125927.0	141014	4.13	3.05	-12.36	0.32	-0.60	0.10*	P	10
225851	125942.6	110438	0.00	3.30	< -14.41	-	-	-	P	11
8114	130025.0	134013	28.92	5.85	-13.19	0.08	-1.27	-1.13	P	9
8166	130352.4	105820	0.00	4.58	< -14.25	-	-	-	P	11
230077	130623.3	102600	27.24	6.83	-13.18	0.10	-1.74	-1.68	P	9

Continued in next page

Continued from previous page

AGC (1)	*R.A.* (*J*2000) hhmmss (2)	*DEC* o ′ ″ (3)	HαEW Å (4)	$\sigma_{\rm EW}$ Å (5)	log F(Hα) erg cm^{-2} s^{-1} (6)	log $\sigma_{\rm F}$ erg cm^{-2} s^{-1} (7)	log SFR M$_\odot$ y^{-1} (8)	log SFR M$_\odot$ y^{-1} (9)	Quality (10)	Fig. (11)
230084	130655.9	144826	11.57	3.32	-13.79	0.12	-2.30	-2.24	P	9
8276	131206.3	052832	9.91	6.37	-13.96	0.28	-2.49	-2.45	P	10
8285	131233.3	071103	0.00	5.81	< -13.58	-	< -2.21	< -2.11	P	11
8298	131319.7	101137	20.04	4.59	-13.15	0.10	-1.63	-1.52	P	9
8345	131652.1	123254	40.74	3.58	-12.46	0.03	-1.07	-0.94	P	9
233627	131953.0	134823	0.00	11.00	< -14.60	-	< -3.09	< -3.05	P	11
8382	132032.2	052426	10.79	5.41	-13.40	0.21	-1.97	-1.88	P	10
8385	132038.1	094714	31.21	5.90	-12.62	0.08	-1.15	-1.00	P	9
8450	132701.2	100322	14.09	4.26	-13.33	0.13	-1.85	-1.77	P	10
230436	133438.0	084737	4.14	4.09	-13.85	0.43	-2.28	-2.18	P	10
8575	133545.5	085806	0.63	11.43	< -13.52	-	< -2.00	< -1.89	P	11
231022	133602.6	081105	6.64	4.43	-14.23	0.29	-2.58	-2.53	P	10
232025	133643.6	083247	0.00	5.33	< -14.15	-	< -2.59	< -2.53	P	11
8616	133732.1	085306	27.74	4.81	-11.20	0.07	0.16	0.54	P	9
8629	133830.6	082632	6.56	4.79	-13.94	0.31	-2.46	-2.39	P	10
233601	133850.8	080629	0.00	28.51	< -14.03	-	< -2.41	< -2.37	P	11
238771	134641.0	063915	8.53	3.89	-14.02	0.20	-2.44	-2.39	P	10
8800	135326.5	051227	0.00	9.91	< -12.97	-	< -1.72	< -1.60	P	11
8821	135411.2	051336	23.52	5.24	-12.44	0.09	-0.84	-0.64	P	9
8831	135458.4	052000	8.56	3.43	-12.55	0.17	-1.02	-0.80	P	9
232141	135504.5	051122	38.59	12.04	-13.65	0.13	-1.92	-1.87	P	9
232142	135609.4	053233	0.00	16.51	< -14.10	-	< -2.56	< -2.52	P	11
8853	135612.0	050052	17.57	4.18	-11.49	0.10	-0.08	0.29	P	9
233571	135741.0	152224	29.97	8.17	-13.53	0.11	-2.02	-1.97	P	10
233718	135843.4	141541	36.33	4.08	-13.57	0.05	-2.06	-2.02	P	10
8995	140447.3	084802	12.71	4.61	-12.95	0.15	-1.43	-1.28	P	10
9020	140631.8	060145	5.67	3.33	-13.00	0.25	-1.64	-1.49	P	10
243852	140704.5	104245	119.86	11.57	-13.27	0.03	-1.67	-1.63	P	9
243881	141750.7	065023	37.53	10.54	-13.69	0.11	-2.08	-2.04	P	10
9169	141944.7	092144	16.75	5.48	-12.73	0.14	-1.21	-1.05	P	10
714055	142044.5	083735	6.62	4.75	-14.21	0.31	-2.57	-2.52	P	10
9202	142210.7	135503	13.62	3.56	-12.51	0.11	-	-	P	9
9225	142424.3	081632	-1.79	6.08	< -13.68	-	< -2.12	< -2.03	P	11
9249	142659.8	084100	48.77	15.31	-12.66	0.13	-1.07	-0.95	P	9
9252	142710.8	050806	28.60	5.43	-13.39	0.08	-1.64	-1.55	P	10
9273	142810.9	133305	35.34	3.87	-12.87	0.04	-1.32	-1.21	P	9
9275	142818.5	134648	21.31	4.52	-12.42	0.09	-0.93	-0.73	P	9
244386	142852.8	123454	9.90	3.27	-14.52	0.14	-3.00	-2.96	P	10
9328	143039.6	071629	21.52	3.54	-12.06	0.07	-0.55	-0.30	P	9
716018	143048.7	070925	21.32	5.40	-14.32	0.11	-2.72	-2.68	P	10
240441	143220.7	095600	15.72	3.68	-13.34	0.10	-1.72	-1.62	P	9
9353	143243.8	095329	24.88	4.52	-11.90	0.08	-0.40	-0.12	P	9
9363	143324.3	042700	40.22	5.24	-11.64	0.05	-0.03	0.28	P	9
9380	143438.8	041537	20.44	7.37	-13.16	0.15	-1.40	-1.28	P	10
9385	143522.8	051636	16.15	7.43	-13.31	0.20	-1.57	-1.46	P	10
9389	143533.2	125427	11.87	4.18	-12.96	0.15	-1.20	-1.01	P	9
9394	143539.9	131012	34.24	4.50	-12.63	0.05	-0.87	-0.70	P	9
240523	143640.9	113437	0.00	30.84	0.00	-	-	-	T	11
9436	143911.0	052147	5.72	4.65	-12.20	0.35	-0.66	-0.32	P	10
714204	143912.4	090805	17.14	4.11	-13.69	0.10	-2.10	-2.05	P	9
249303	144119.2	074735	44.80	13.17	-13.32	0.12	-1.48	-1.40	P	9
9483	144257.9	045324	12.15	3.05	-12.53	0.11	-0.88	-0.66	P	9
9485	144302.8	044554	23.86	6.87	-13.24	0.12	-1.46	-1.35	P	10
242618	144329.2	043153	19.27	10.09	-13.63	0.22	-1.81	-1.73	P	10
9500	144521.4	075145	5.65	4.37	-13.72	0.33	-1.97	-1.85	P	10
242016	144624.3	141247	-1.31	47.63	< -13.23	-	< -1.45	< -1.39	P	11
240700	144728.4	124553	84.26	4.57	-12.88	0.02	-1.06	-0.96	P	9
9535	144842.5	122724	17.78	5.85	-12.95	0.14	-1.23	-1.01	P	9
245076	145243.5	114020	26.79	14.85	-13.84	0.23	-2.08	-2.04	P	10
241727	145837.8	064630	32.47	4.01	-13.22	0.05	-1.46	-1.36	P	9
257898	152059.4	121052	0.05	3.78	< -14.64	-	< -3.11	< -3.07	P	11
9824	152156.5	050412	19.34	4.63	-11.67	0.10	-0.15	0.16	P	9
9830	152300.8	043145	5.74	4.39	-13.64	0.33	-1.85	-1.73	P	10
258405	152411.4	072918	64.85	5.49	-12.99	0.03	-1.42	-1.37	P	10
9845	152605.4	091216	17.19	3.91	-13.24	0.10	-1.43	-1.31	P	9
252085	153139.0	153532	59.45	8.86	-13.05	0.06	-3.24	-3.20	P	10
9895	153343.1	150025	28.26	9.32	-12.37	0.14	-0.67	-0.44	P	9
9902	153433.1	150759	59.45	31.73	-13.58	0.22	-1.75	-1.71	P	10
257920	153446.6	122650	63.49	4.63	-13.36	0.03	-	-	P	9
9908	153458.6	114500	23.54	9.19	-12.53	0.17	-0.79	-0.55	P	9
257921	153507.9	122013	30.74	21.06	-13.89	0.29	-2.27	-2.23	P	10
9915	153523.2	120250	18.42	5.76	-12.21	0.13	-0.52	-0.24	P	9
9935	153736.2	055825	24.90	6.81	-11.90	0.11	-0.37	-0.11	P	10

Continued in next page

Continued from previous page

AGC (1)	*R.A.* (*J*2000) hhmmss (2)	*DEC* $^{o}\ '\ ''$ (3)	HαEW Å (4)	$\sigma_{\rm EW}$ Å (5)	log F(Hα) erg cm^{-2} s^{-1} (6)	log $\sigma_{\rm F}$ erg cm^{-2} s^{-1} (7)	log SFR M$_\odot$ y^{-1} (8)	log SFR M$_\odot$ y^{-1} (9)	Quality (10)	Fig. (11)
9941	153821.9	125738	0.00	40.09	$<$ -13.13	-	$<$ -1.31	$<$ -1.22	P	11
9943	153830.0	121110	21.90	3.47	-11.81	0.07	-0.09	0.25	P	9
257927	153836.7	133103	9.05	4.70	-14.22	0.22	-	-	P	10
257929	153857.5	123256	11.25	3.34	-13.90	0.13	-2.38	-2.33	P	9
9987	154253.0	141354	39.98	9.34	-12.18	0.10	-0.85	-0.67	P	9
9991	154323.9	142608	31.16	15.80	-12.95	0.21	-1.15	-1.01	P	10
10014	154544.0	123038	5.59	4.30	-13.86	0.33	-2.41	-2.34	P	10
10023	154609.8	065353	15.80	4.52	-13.26	0.12	-1.67	-1.58	P	9
10083	155413.8	143603	30.76	9.90	-11.92	0.14	-0.24	0.03	P	9
252891	155636.8	061139	0.00	41.75	$<$ -13.67	-	$<$ -1.79	$<$ -1.73	P	11
258430	155955.5	065303	62.46	9.60	-13.89	0.06	-	-	P	10
261969	160602.2	083025	27.08	4.50	-13.35	0.07	-	-	P	9
261313	160641.0	063451	23.92	4.33	-13.09	0.08	-	-	P	9
10219	160817.0	073216	12.81	4.33	-12.81	0.14	-	-	P	12
268216	161220.5	063237	23.74	8.57	-14.03	0.15	-	-	P	12
214319+	112607.8	040345	33.35	3.86	-13.56	0.05	-	-	P	-
213169+	113517.3	045725	14.0	3.37	-14.21	0.1	-	-	P	-

Concluded from previous page